RESEARCH MEMORANDUM

for the

Bureau of Aeronautics, Department of the Navy

SUMMARY OF THE LIFT, DRAG, AND STABILITY OF 1/10-SCALE ROCKET-BOOSTED MODELS OF THE MCDONNELL XF3H-1 AIRPLANE FOR A MACH NUMBER RANGE OF 0.6 TO 1.4 AS AFFECTED BY THE OPERATION OF EXTENSIBLE ROCKET RACKS

TED NO. NACA DE 351

By Norman L. Crabill and John C. McFall, Jr.

Langley Aeronautical Laboratory
Langley Field, Va.

NATIONAL ADVISORY COMMITTEE
FOR AERONAUTICS

WASHINGTON

JAN 26 1954

ERRATA NO. 1

NACA RM SL54A18

SUMMARY OF THE LIFT, DRAG, AND STABILITY OF 1/10-SCALE ROCKET-BOOSTED MODELS OF THE MCDONNELL XF3H-1 AIRPLANE FOR A MACH NUMBER RANGE OF 0.6 TO 1.4 AS AFFECTED BY THE OPERATION OF EXTENSIBLE ROCKET RACKS
TED NO. NACA DE 351
By Norman L. Crabill and John C. McFall, Jr.

January 26, 1954

Page 8, line 13: The sentence beginning on this line should be changed to read as follows:

The corrected values of C_{n_β} are about 16 percent less than those obtained previously from the first test (ref. 1) wherever the scatter of that data is small.

Figure 14: This figure should have a correction made by replacing the lower plot with the following corrected plot for part (b):

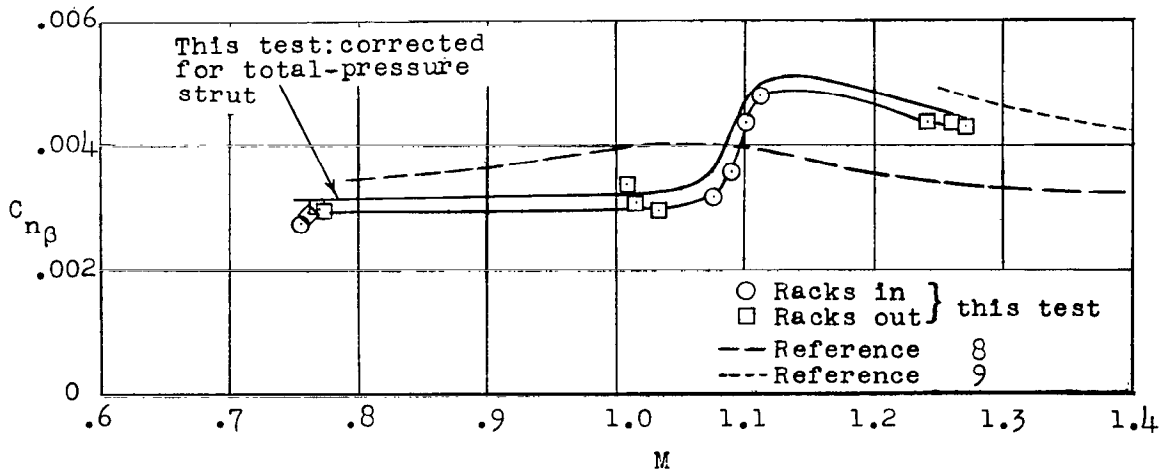

Figure 14 (b) Static-stability derivative C_{n_β}.

NACA RM SL54A18

NATIONAL ADVISORY COMMITTEE FOR AERONAUTICS

RESEARCH MEMORANDUM

for the

Bureau of Aeronautics, Department of the Navy

SUMMARY OF THE LIFT, DRAG, AND STABILITY OF 1/10-SCALE ROCKET-BOOSTED MODELS OF THE MCDONNELL XF3H-1 AIRPLANE FOR A MACH NUMBER RANGE OF 0.6 TO 1.4 AS AFFECTED BY THE OPERATION OF EXTENSIBLE ROCKET RACKS

TED NO. NACA DE 351

By Norman L. Crabill and John C. McFall, Jr.

SUMMARY

A flight investigation using two rocket-boosted 1/10-scale models of the McDonnell XF3H-1 airplane has been conducted by the National Advisory Committee for Aeronautics to determine the aerodynamic effects of operating internally stowed extensible rocket racks during transonic flight. Results from the flight of the second model are presented here for the first time; some comparisons with the first test are included. With the exception of the effect on drag, operation of the racks generally had only a small effect on the aerodynamic characteristics of the model. A region of apparently variable dynamic longitudinal stability between a Mach number of 1.10 and 1.27 found in the test of the first model of this program and attributed to the presence of the rocket racks was repeated over a somewhat smaller Mach number range. The supersonic flutter encountered in the test of the second model was incidental to the purpose of the test and is not likely to appear on the full-scale airplane.

INTRODUCTION

At the request of the Navy Department, Bureau of Aeronautics, the NACA has performed an experimental investigation of the effects of the

extension of internally stowed rocket racks on the lift, drag, stability, and trim of two 1/10-scale rocket-boosted models of the McDonnell XF3H-1 airplane. The results of the second (and last) test are reported herein for the first time. In addition, some of the more important results obtained from the previous test are presented.

The models were supplied by the McDonnell Aircraft Corporation, and the flights were made at the Langley Pilotless Aircraft Research Station at Wallops Island, Va.

SYMBOLS

a_l acceleration parallel to fuselage center line at center of gravity, positive toward tail, ft/sec^2

a_n acceleration perpendicular to fuselage center line at center of gravity, positive upward, ft/sec^2

a_t acceleration perpendicular to plane of symmetry, near center of gravity, positive toward right wing tip, ft/sec^2

b wing span, ft

C_D total drag coefficient, $C_N \sin \alpha + C_C \cos \alpha$

C_L total lift coefficient, $C_N \cos \alpha - C_C \sin \alpha$

C_m pitching-moment coefficient, positive for a moment tending to raise nose, $\frac{\text{Pitching moment}}{qS_{wing}\bar{c}}$

$C_{m_{\dot{\alpha}}} = \frac{\partial C_m}{\partial \frac{\dot{\alpha}\bar{c}}{2V}}$

$C_{m_q} = \frac{\partial C_m}{\partial \frac{\dot{\theta}\bar{c}}{2V}}$

C_n yawing-moment coefficient, $\frac{\text{Yawing moment}}{qS_{wing}b}$

C_C chord-force coefficient, $\frac{a_l}{g}\frac{W}{qS_{wing}}$

[redacted]

C_N normal-force coefficient, $\frac{a_n}{g}\frac{W}{qS_{wing}}$

C_Y lateral-force coefficient, $\frac{a_t}{g}\frac{W}{qS_{wing}}$

$\bar{c}$ wing mean aerodynamic chord, ft

f frequency, cps

g acceleration due to gravity, 32.2 ft/sec^2

I_Y mass moment of inertia of model about transverse axis, slug-ft^2

I_Z mass moment of inertia of model about axis perpendicular to longitudinal principal axis and transverse axis, slug-ft^2

l_X horizontal distance from center of gravity of model to center of rocket racks, ft

l_Z vertical distance from center of gravity of model to centroid of exposed frontal area of rocket rack, ft

M free-stream Mach number

M3,M4,M7 rocket-rack modifications

P period of motion, sec

p free-stream static pressure, lb/sq ft

q dynamic pressure, $\frac{\gamma}{2}pM^2$

m/m_o mass-flow ratio

$q = \frac{d\theta}{dt}$

R Reynolds number based on wing mean aerodynamic chord

S wing area, sq ft

T time, sec

[redacted]

V	free-stream velocity, ft/sec
W	weight of model, lb
θ/L	wing twist in free-stream direction due to a unit load at various span loading stations, radians/lb
y	distance from model center line, ft
η	distance from model center line, $y/\frac{b}{2}$, semispans
α	angle of attack of fuselage center line, positive nose up, deg
$\dot{\alpha} = \frac{1}{57.3}\frac{d\alpha}{dt}$	
β	angle of sideslip, positive for relative wind coming from right, deg
δ	angular deflection, deg
γ	ratio of specific heats at atmosphere, 1.4
θ	angle of fuselage center line relative to horizontal, positive nose up, radians

Subscripts:

min	minimum
RR	rocket racks
s	horizontal stabilizer
t	trim
av	average

Derivatives with respect to a quantity are indicated as shown in the following example: $C_{m_{C_L}} = \frac{dC_m}{dC_L}$

Increments are denoted by Δ, for example:

ΔC_{L_t}	increment in trim lift coefficient

[redacted]

DESCRIPTION OF MODEL AND INSTRUMENTATION

Model

Physical characteristics of the model in this investigation are presented in table I and by drawings and photographs in figures 1 and 2. For this model the center of gravity was at 27.9 percent of the mean aerodynamic chord and the horizontal stabilizer was set at -2.3° relative to the wing. As in the model of reference 1, the ducts were blocked completely just inside the inlet and at the jet exit. Additional model description and construction details may be found in reference 1. The model was subjected to vibrations of known frequency (as in ref. 1) and the results are presented in figure 3. Measured wing influence coefficients are shown in figure 4.

Instrumentation

The model contained an NACA telemetering system which transmitted continuous information to the ground receiving station during the flight. In addition to the accelerometers (whose locations are indicated in fig. 3) the instrumentation used in this investigation consisted of pressure cells measuring total and static pressure, rocket-rack position indicator, and an NACA vane-type angle-of-attack indicator (ref. 2).

The ground instrumentation of this test was the same as that described in reference 1.

TEST AND METHOD OF ANALYSIS

The test technique employed was similar to that described in references 1 and 3. A photograph of the model on the launcher is shown as figure 2(c). The Reynolds number, based on the wing mean aerodynamic chord, varied, as shown in figure 5, between 4.1×10^6 at $M = 0.62$ and 11.1×10^6 at $M = 1.37$. A time history of the principal quantities is shown as figure 6. The results presented in this paper were derived from this time history by the method of reference 3, except where otherwise noted. The axis system used in the analysis is shown in figure 7.

RESULTS AND DISCUSSION

Flutter

Almost immediately after the model separated from the booster, a high-frequency oscillation became visible on the telemeter traces of the

[redacted]

angle-of-attack indicator, the nose normal accelerometer, the center-of-gravity normal and longitudinal accelerometers, and the normal accelerometer at the tail. A portion of one of the telemeter records showing some of these traces with the flutter oscillation superposed is shown as figure 8. The frequency of the oscillation (fig. 9(a)) was the same on all five traces and varied from 200 cps at $M = 1.37$ to 145 cps near $M = 1.0$. The average half amplitudes of the accelerations involved are shown in figure 9(b) as ΔC_N and ΔC_C to show the manner in which the oscillation damped as a Mach number of one was approached. The resonant frequencies and the corresponding nodal lines of the model components, determined before the flight by mechanically shaking the model are shown in figure 3. The complex nodal pattern on the wing derives from its construction, shown in figure 1(c).

From the character of the oscillations, shown in figure 8, it was concluded that the phenomenon was flutter. However, other rocket-model tests of wings scaled to represent the airplane structurally as well as aerodynamically, having much lower frequencies in both bending and torsion, indicated no wing flutter for the airplane up to at least $M = 1.5$ (these results are as yet unpublished). The occurrence of flutter in the present test was purely incidental to the purpose of the test and evidently represents a borderline case, since a previous test of a model almost exactly similar to this one, but trimmed to fly at higher angles of attack, did not flutter. Calculations performed by the McDonnell Aircraft Corporation indicate that, for these models, a type of flutter involving a chordwise bending of the trailing edge about the rear edge of the spar (fig. 1(c)) would be possible over the range of speeds and frequencies observed in this test. Hence, it is concluded that the flutter observed in this test is peculiar to this model and is not likely to appear on the full-scale airplane.

Immediately after booster-model separation the angle-of-attack indicator was apparently damaged by vibration induced by the flutter. (Note the existence of a nodal line at a frequency of 190 cps at the base of the angle-of-attack sting, fig. 3.) Hence, angle-of-attack data were not used in this analysis. Throughout the flutter, the correct values of the accelerations corresponding to the model short-period longitudinal and lateral modes of motion were assumed to be the average between the envelopes through the peaks.

Static Longitudinal Stability

Angle-of-attack stability.- The period of the longitudinal motion, shown in figure 10(a), was obtained from the time history of the normal-force coefficient. By using the method of reference 3 these values of period were converted to the static-stability derivative C_{m_α} (fig. 10(b)), and compared with the rocket model of reference 1 and wind-tunnel tests

reference 4. For the model in this investigation slightly less static stability is indicated than in the wind-tunnel tests. Data from both sources agreed in the general variation of C_{m_α} with Mach number.

Aerodynamic-center location.- Values of pitching-moment coefficient obtained with two accelerometers by the method of reference 5 were plotted against normal-force coefficient in figure 11 for two supersonic Mach numbers with racks in and one supersonic Mach number with racks out. Data from reference 1 at two supersonic Mach numbers are also presented in figure 11 for a different stabilizer setting and with racks only partially out. The slopes from these data are shown in figure 12 as aerodynamic-center location. Also the C_{m_α} of figure 10 was used with the C_{l_α} of reference 4 to determine the aerodynamic-center location. The results indicate a rearward shift of about 13 percent mean aerodynamic chord between $M = 0.85$ and 1.0, followed by a more gradual shift up to the test limit, $M = 1.34$.

A similar variation of aerodynamic-center location with Mach number is reported for this configuration in reference 4 (fig. 12). However both rocket models (this test and ref. 1) indicated somewhat less stability than the wind-tunnel references but slightly more than the flight data of reference 6.

Dynamic Longitudinal Stability

Since the effect of the racks on the longitudinal motion was small, damping data could be obtained only from the separation oscillation, $t \approx 3.3$ seconds, figure 6. The sum of the derivatives C_{m_q} and $C_{m_{\dot\alpha}}$ (fig. 13) determined for this oscillation agrees with the result of reference 1. The estimated value, computed by the methods outlined in reference 7 is about 80 percent of the actual value near $M = 1.3$.

In several instances, the small-amplitude longitudinal motions were irregular in frequency and damping. At $t \approx 3.85$ seconds, $M = 1.23$ (fig. 6), this irregular nature of the motion was apparent; however, the motion damped when the rocket racks retracted, $t = 4.40$ seconds, $M = 1.14$. This apparently variable dynamic and static stability occurred in the test of a similar model, (ref. 1) under similar conditions over a slightly greater Mach number range, $M = 1.10$ to 1.27. Either the rocket racks are capable of producing some interference effect or turbulence of a continuous nature at least between $M = 1.10$ and 1.27, or inertial or aerodynamic coupling occurred between the lateral and longitudinal modes in both instances. The turbulence effect seems to be more likely in view of the damping when the racks closed. If it is a turbulence effect, the resulting motion of the model is the dynamic response of the model to a continuous disturbance. The effect of such turbulence on the dynamic

stability of the full-scale airplane at the same altitude (about 2,000 ft) would be less pronounced because of dynamic considerations.

The causes of the other irregularities occurring in the longitudinal motion (e.g., $t = 5.7$, 6.8, and 8.4) cannot be defined by the methods of analysis given in reference 3.

Static Directional Stability

The period of the lateral motion (fig. 14(a)) was determined from the time history of the lateral-force coefficient (fig. 6) at those times during which the lateral motion was sinusoidal. The directional static-stability derivative C_{n_β} equivalent to these period values is shown in figure 14(b). In order to approximate the airplane more closely, a correction was applied to the faired C_{n_β} curve to account for the fin effect of the total-pressure tube strut (fig. 1). The corrected values of C_{n_β} agree closely with those obtained previously from the first test (ref. 1) wherever the scatter of that data is small. Although the preliminary estimate of reference 8 predicts only a small variation with Mach number, the results of the present test are characterized by an abrupt increase between $M = 1.07$ and $M = 1.13$. The level of the supersonic data of reference 9 and this test is much larger than the estimate of reference 8.

Trim

Trim normal-force coefficient.- The trim normal-force coefficient, shown as a function of Mach number in figure 15 for rocket racks in and out, displayed a moderate nose-down tendency from $M \approx 0.90$ to 0.96 and a milder pitchup characteristic from $M = 0.97$ to 1.1. The trim estimated from reference 5 for this model (with no air flow through the ducts) indicated a much higher trim at subsonic speeds, with a moderate pitchup tendency centered about $M = 0.80$. The trim for large mass flow through the ducts indicates such a peak at $M = 0.87$, followed by a gradual nose-down tendency throughout the remainder of the transonic speed range.

Pitching-moment coefficient at zero lift.- The trim lift of the model with racks in was used with the static stability obtainable from figure 12 to calculate the pitching-moment coefficient at zero lift. This quantity was also determined directly from figure 11 for the separation oscillation. These values of $(C_m)_{C_{L=0}}$ in figure 16 are considerably smaller than those reported in reference 4 and show an increase of about 0.01 in $(C_m)_{C_{L=0}}$ in going from subsonic to supersonic speeds.

[redacted]

Stabilizer effectiveness for trim.- By comparing the values of C_{N_t} obtained in this test with the trim obtained in reference 1 (see fig. 15), the derivative $\Delta C_{N_t}/\Delta\delta_s$ has been determined. (Since the rocket racks did not fully close in the first test, the comparison was made for the racks-out condition.) These values of $\Delta C_{N_t}/\Delta\delta_s$ (fig. 17) are slightly larger than those derived from the data of reference 4, due, probably, to the lower static stability obtained in this test.

Drag

Since angle-of-attack data were not available, no actual drag data can be presented. However, in the lift range being considered, the chord-force coefficient does not vary much with angle of attack, and the actual values of chord-force coefficient shown in figure 18 may be cautiously used as minimum drag coefficients. In order to compare these data with the results of tunnel tests of models having faired-over inlets, these values have been corrected for base drag and for the effects of the blocked inlets as described in reference 1. These corrected results agree with data from references 1 and 9 below $M = 1.1$, but at $M = 1.3$, the corrected result is about $\Delta C_D = 0.009$ higher than the level established by these other tests.

Effect of Rocket Racks on Aerodynamic Characteristics of the Model

Effect of rocket racks on drag.- The effect of the rocket racks on chord-force coefficient was determined by plotting C_C as a function of $C_N{}^2$ for a short interval before and after the movement of the rocket racks and then determining the increment between the resulting two straight lines (fig. 19). Since the angle of attack is small and the change in lift due to the presence of the racks is small, $\Delta C_{D_{RR}} \approx \Delta C_{C_{RR}}$. This drag increment, 0.006 at subsonic speeds, becomes a minimum at about $M = 1.0$ and increases to about 0.0082 at $M = 1.3$ (fig. 20). The results of reference 1 are in general agreement except at $M = 1.27$, where reference 1 indicates an increment of $\Delta C_{D_{RR}} = 0.0117$. Since this value was obtained by a process of extrapolation designed to account for a rack movement over only the last half of its intended range (see ref. 1), its accuracy is questionable. The results of tests of rack configurations M3 and M7 from references 10 and 11, respectively, are also shown in figure 20. Thus, the tests on all the rack configurations indicate that the increment in drag coefficient is considerable over most of the Mach number range.

Effect of rocket racks on trim.- The trim normal-force coefficient shown in figure 15 for rocket racks in and for rocket racks out was used to determine the increment in trim normal-force coefficient due to the presence of the rocket racks. This quantity, shown in figure 21, has a maximum value of -0.06 at $M = 0.98$ and becomes positive above $M = 1.15$. Tests on rack configurations M3, M4, and M7 (ref. 5) indicate a similar variation; however, these wind-tunnel tests indicate a larger negative effect.

Effect of rocket racks on pitching moment.- An indication of the effect of rocket racks on the pitching-moment coefficient at constant lift coefficient, shown in figure 22, was obtained by use of the following relationship:

$$\left(\Delta C_{m_{RR}}\right)_{C_L=\text{Constant}} = \left(\Delta C_{m_{RR}}\right)_{C_L} = -C_{m_{C_L}} \Delta C_{N_{t_{RR}}}$$

where $C_{m_{C_L}}$ was taken from the heavy dashed line in figure 12 (this test), and $\Delta C_{N_{t_{RR}}}$ from figure 21 (this test).

Comparison in figure 22 with data from reference 4 shows the variation of the effect of racks on pitching moment with Mach number to be well-defined. The one point obtained from figure 11 indicates that the level of the computed increment in pitching moment is of the right order of magnitude for the present test. A reversal of effect occurs at $M = 1.15$ which is a lower Mach number than indicated by the wind-tunnel references.

Effect of rocket racks on lift.- The effect of rocket racks on lift coefficient at a constant angle of attack is shown in figure 23. These values were computed using the following relationship:

$$\left(\Delta C_{L_{RR}}\right)_{\alpha} = \frac{\left(\Delta C_{m_{RR}}\right)_{C_L} + \Delta C_{C_{RR}} \frac{l_Z}{\bar{c}}}{\frac{l_X}{\bar{c}} - C_{m_{C_L}}}$$

Values of $\Delta C_{C_{RR}}$, $C_{m_{C_L}}$, and $\left(\Delta C_{m_{RR}}\right)_{C_L}$ were obtained from figures 20, 12, and 22 (this test), respectively. The lift was assumed to be concentrated at the center of the rocket racks in determining the distance $l_X/\bar{c}$. Data from tests of similar racks (refs. 9 and 11) are also shown in figure 23. As could be expected from the results of figure 22, the lift due to the racks is greater at supersonic speeds than the tunnel tests indicated.

[redacted]

SUMMARY OF RESULTS

The principal results derived from an analysis of the accelerations of a 1/10-scale model of the McDonnell XF3H-1 airplane equipped with internally stowed extensible rocket racks which were pulsed in a square-wave program while the model was decelerating in free flight from a Mach number M of 1.37 to 0.62 are:

1. The change in trim normal-force coefficient due to the extension of the rocket racks was greatest, $\Delta C_{N_{t_{RR}}} = -0.06$, at $M = 0.98$; above $M = 1.15$ it was positive.

2. The increment in pitching-moment coefficient due to the extension of the racks at constant lift coefficient was greatest, $\left(\Delta C_{m_{RR}}\right)_{C_L} = -0.012$, at $M = 1.00$; above $M = 1.15$ it was positive.

3. The increment in drag coefficient due to the racks was considerable over most of the Mach number range. It varied from 0.006 at subsonic speeds to about 0.0082 at $M = 1.3$.

4. A region of variable dynamic longitudinal stability was experienced between $M = 1.14$ and 1.23 and is attributed to the presence of the rocket racks since the irregular longitudinal motion ceased when the racks closed, and the same phenomenon was observed over a slightly greater Mach number range in a previous test.

5. The effect of the rocket racks on lift coefficient at constant angle of attack was small; in fact, the maximum increment, near $M = 1.0$, was only $\left(\Delta C_{L_{RR}}\right)_{\alpha} = -0.017$. It became positive above $M = 1.135$.

6. The supersonic flutter experienced was incidental to the purpose of the test, and is not likely to appear on the full-scale airplane.

7. The rearward shift of the aerodynamic center amounted to 13 percent between $M = 0.85$ and $M = 1.0$. In general the static longitudinal stability was found to be somewhat less than wind-tunnel tests of similar models indicated.

[redacted]

8. The directional static-stability derivative C_{n_β} increased abruptly between $M = 1.07$ and 1.13.

Langley Aeronautical Laboratory,
National Advisory Committee for Aeronautics,
Langley Field, Va., January 5, 1954.

Norman L. Crabill

Norman L. Crabill
Aeronautical Research Scientist

John C. McFall, Jr.

John C. McFall, Jr.
Aeronautical Research Scientist

Approved: Joseph A. Shortal

Joseph A. Shortal
Chief of Pilotless Aircraft Research Division

mhg

[redacted]

REFERENCES

1. Crabill, Norman L.: The Effects of Extensible Rocket Racks on Lift, Drag, and Stability of a 1/10-Scale Rocket-Boosted Model of the McDonnell XF3H-1 Airplane for a Mach Number Range of 0.60 to 1.34 – TED No. NACA DE 31. NACA RM SL53F15, Bur. Aero., 1953.

2. Mitchell, Jesse L., and Peck, Robert F.: An NACA Vane-Type Angle-of-Attack Indicator for Use at Subsonic and Supersonic Speeds. NACA RM L9F28a, 1949.

3. Gillis, Clarence L., Peck, Robert F., and Vitale, A. James: Preliminary Results From a Free-Flight Investigation at Transonic and Supersonic Speeds of the Longitudinal Stability and Control Characteristics of an Airplane Configuration With a Thin Straight Wing of Aspect Ratio 3. NACA RM L9K25a, 1950.

4. Rousseau, W. A.: Model XF3H-1 – Basic Wind Tunnel Longitudinal Stability Data – Mach Nos. .18 Thru 1.73. Rep. No. 2101 (Contract NOa(s)-10260), McDonnell Aircraft Corp., May 15, 1951.

5. Vitale, A. James: Effects of Wing Elasticity on the Aerodynamic Characteristics of an Airplane Configuration Having 45° Sweptback Wings As Obtained From Free-Flight Rocket-Model Tests at Transonic Speeds. NACA RM L52L30, 1953.

6. Sohn, R. F., Grose, G. G., Allen, D. W., Lacey, T. R., and Gillooly, R. P.: Model XF3H-1 – Analysis of Preliminary Flight Test Results – Revision Number 1. Rep. No. 2496 (Contract NOa(s)-10260), McDonnell Aircraft Corp., Aug. 29, 1952.

7. Gillis, Clarence L., and Chapman, Rowe, Jr.: Summary of Pitch-Damping Derivatives of Complete Airplane and Missile Configurations As Measured in Flight at Transonic and Supersonic Speeds. NACA RM L52K20, 1953.

8. Clark, D. D.: Model XF3H-1 – Summary of Preliminary Lateral-Directional Dynamic Stability Calculations. Rep. No. 1544 (Contract NOa(s)-10260), McDonnell Aircraft Corp., Jan. 20, 1950.

9. Krenkel, A. R.: Model XF3H-1 – Supersonic Wind Tunnel Tests at O.A.L. on 1.5% and 4.5% Scale Models. Rep. No. 1685 (Contract NOa(s)-10260), McDonnell Aircraft Corp., May 19, 1950.

10. Pliske, D. R.: Model XF3H-1 – Summary of Transonic Wind Tunnel Tests on a 2% Scale Bump Model – Series I. Rep. No. 1545 (Contract NOa(s)-10260), McDonnell Aircraft Corp., Mar. 1, 1950.

[redacted]

11. Von Tungeln, F. W.: Report on High-Speed Wind Tunnel Tests of a 0.10-Scale Model of the McDonnell XF3H-1 Airplane. CWT Rep. 152, Southern Calif. Cooperative Wind Tunnel, Nov. 3, 1950.

[redacted]

TABLE I.- PHYSICAL PROPERTIES AND DIMENSIONS

Dimensions	Wing	Stabilizer	Fin
Span, in.	42.40	17.40	8.55
Mean aerodynamic chord, in.	14.63	6.00	7.99
Area, total, sq ft	4.15	0.700	0.454
Aspect ratio	3	3	1.118
Taper ratio	0.5	0.5	0.5
Incidence, deg	[a]2.20	[b]-2.30	[a]-0.10
Twist, deg	0	0	0
Dihedral, deg	0	0	----
Airfoil section at -			
Root	NACA 0009-1.16 38/1.14 mod.	NACA 0007-1.16 38/1.14 mod.	
Tip	NACA 0007-1.16 38/1.14 mod.		
Sweepback of c/4 line, deg	45	45	45
Location of c/4 of M.A.C.:			
Longitudinal, fuselage station, in.	32.97	63.36	60.93
Vertical, distance from bottom of fuselage, in.	2.52	7.60	12.59
Lateral, spanwise distance from fuselage center line, in.	9.38	3.81	0
Fuselage base area, sq ft	0.0767		

[a]Relative to fuselage center line.

[b]Relative to wing-chord plane.

Mass characteristics:	
Weight, lb	118.95
Wing loading, lb/sq ft	28.66
Center-of-gravity location:	
Longitudinal, percent M.A.C. behind L.E.	27.9
Vertical, percent M.A.C. above center line	2.2
Moments of inertia:	
I_Y, slug-ft^2	5.40
I_Z, slug-ft^2, estimated	6.07

[redacted]

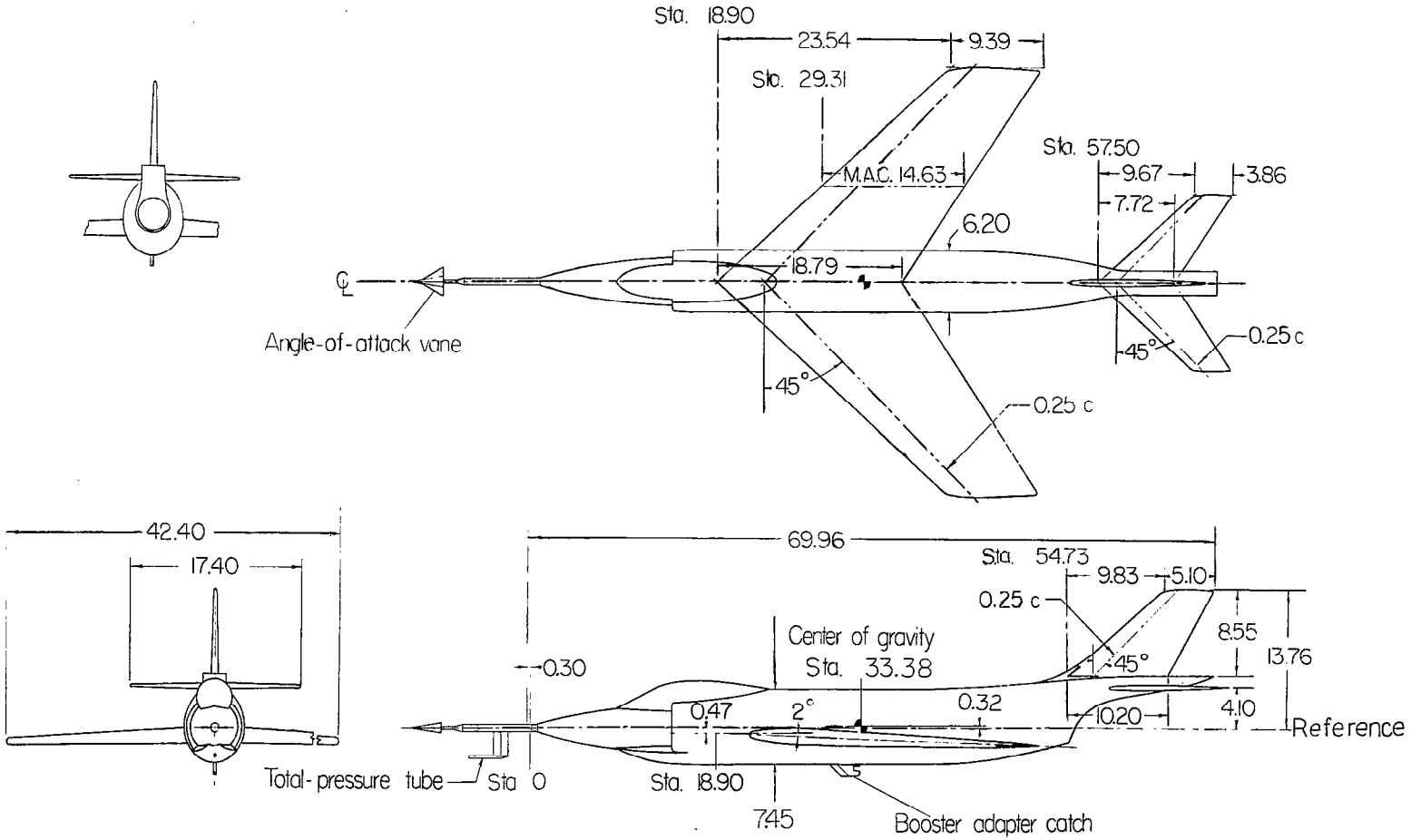

(a) General arrangement.

Figure 1.- Drawings of the 1/10-scale model of the McDonnell XF3H-1 airplane.

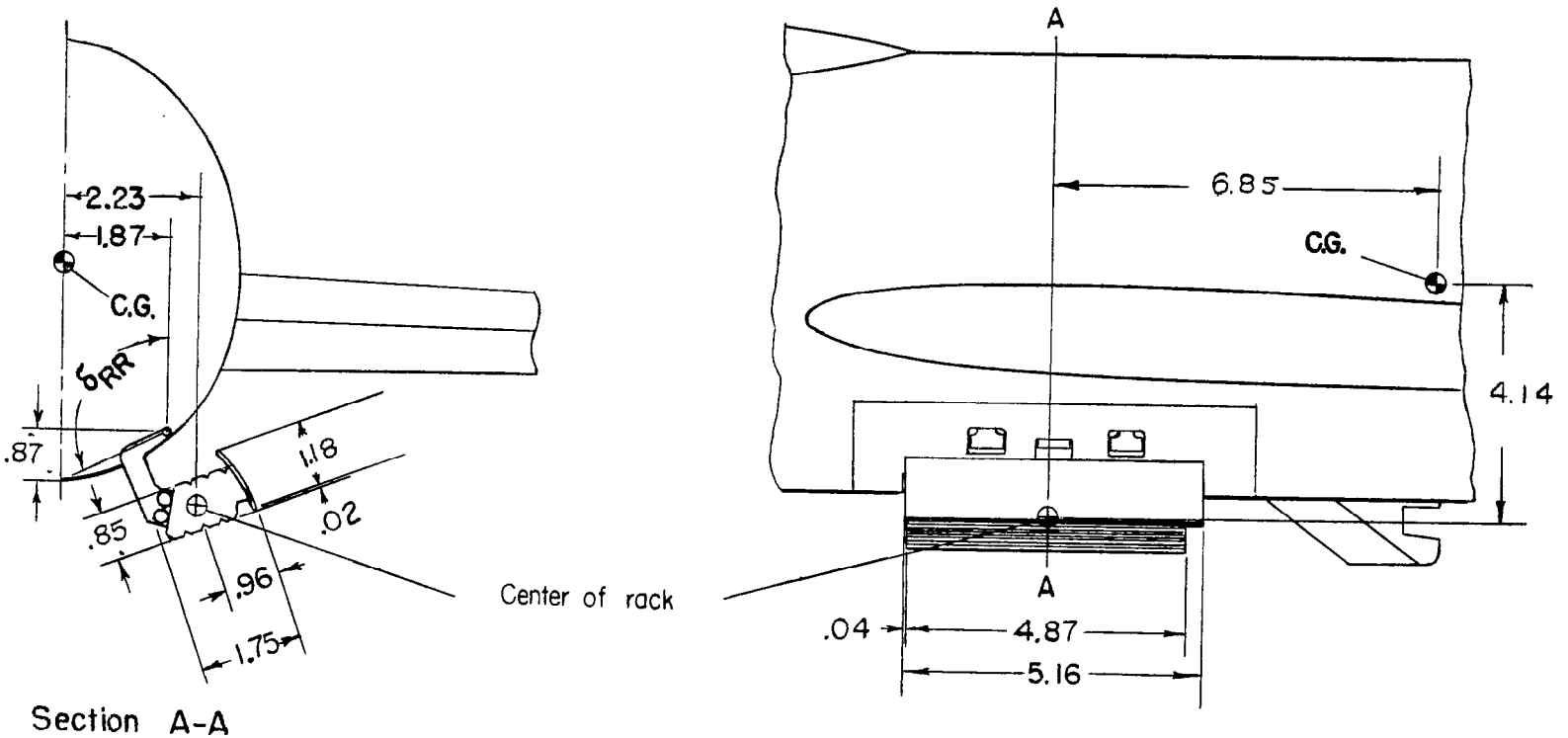

Rocket – Rack Design Conditions

Position	Extension	Frontal area (total)
Closed	0	0
Open	114.3°	0.022 ft^2

(b) Rocket rack detail.

Figure 1.- Continued.

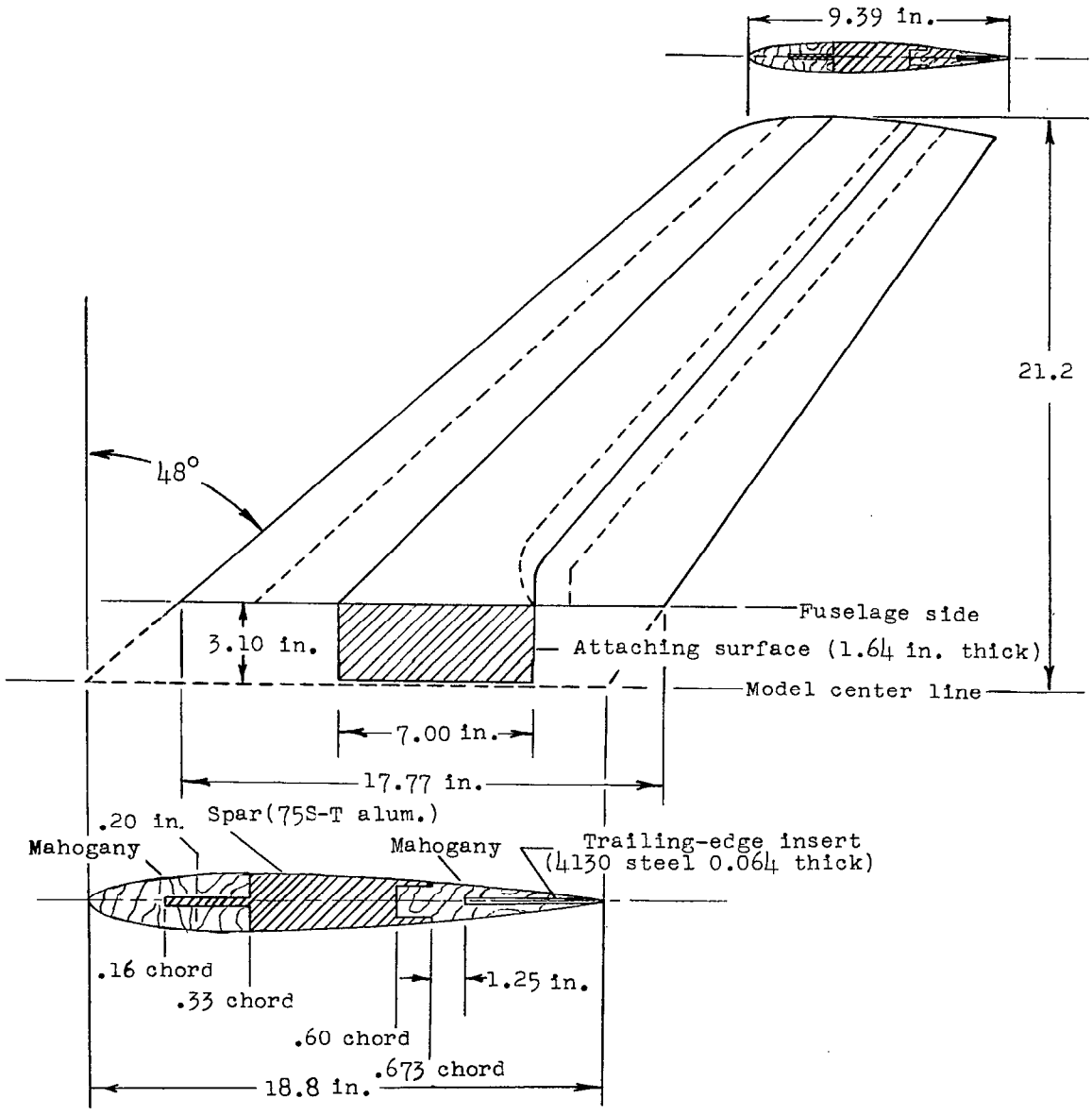

(c) Wing detail.

Figure 1.- Concluded.

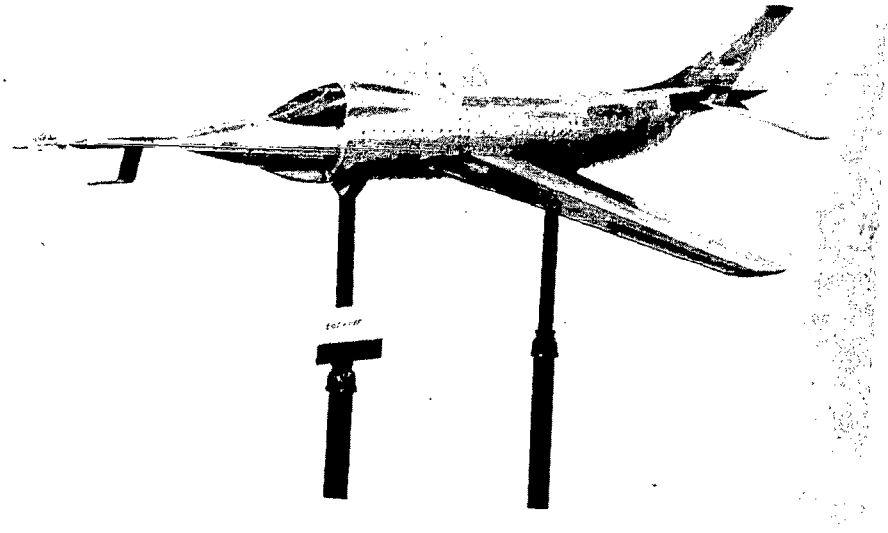

L-80492

(a) Side view.

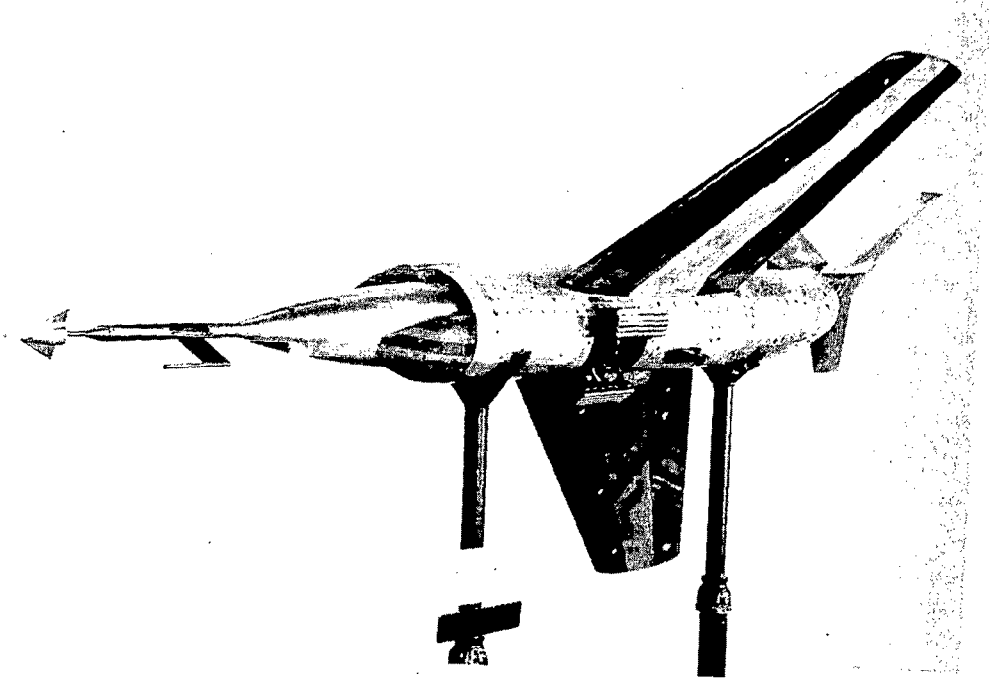

L-80491

(b) Bottom view.

Figure 2.- Photographs of model.

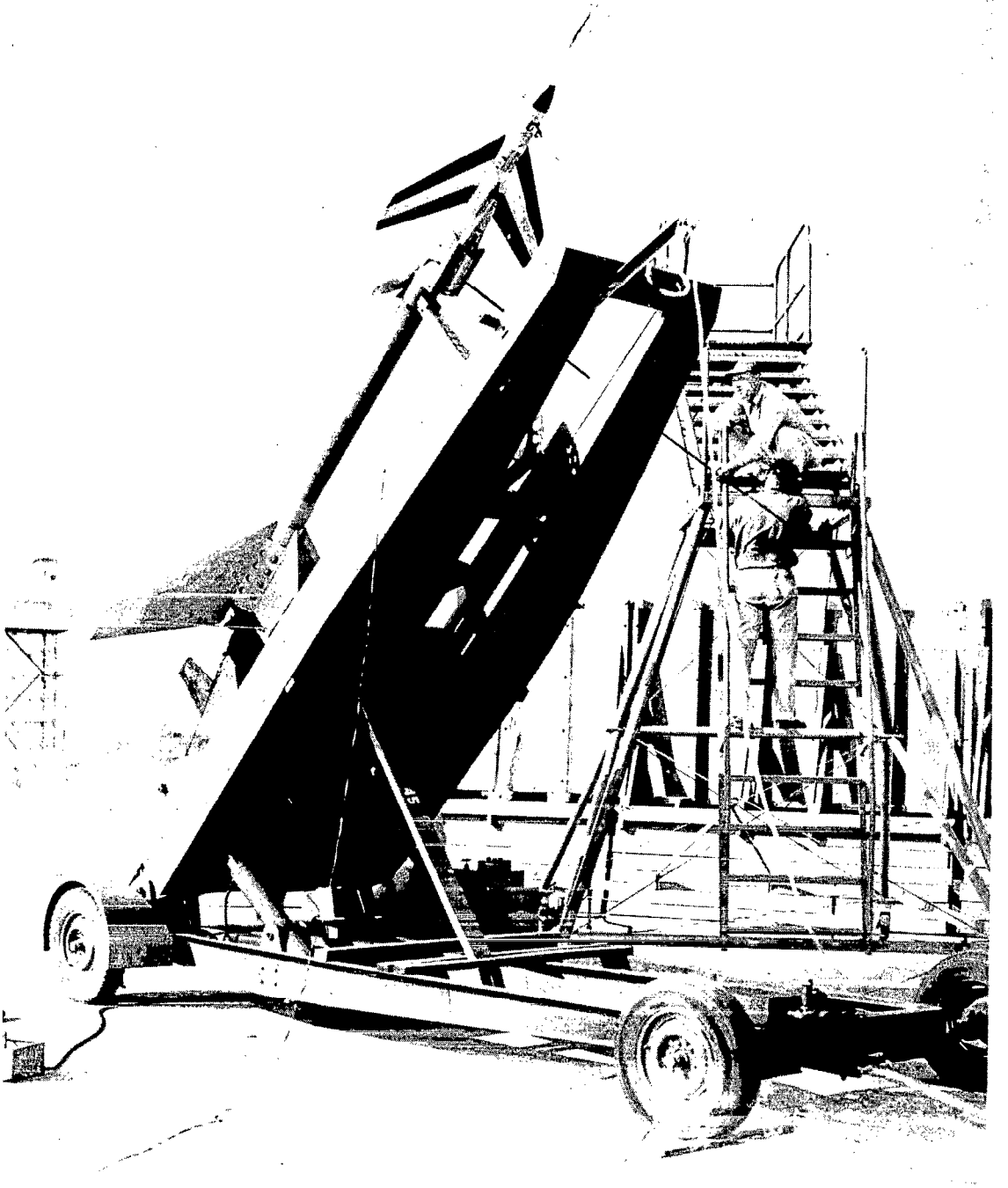

L-80651

(c) Model on launcher.

Figure 2.- Concluded.

FREQUENCIES OBSERVED ON TELEMETER TRACES

WHEN COMPONENTS WERE STRUCK

	$a_{N_{nose}}$	$a_{N_{cg}}$	$a_{N_{tail}}$	a_t	a_l
Left wing	86.2	110	84.6	157	85.5
Right wing	118	115	87	102	-
Vert. fin	-	-	87.3	93.9	-
Right stab.	115	115	87	104	-

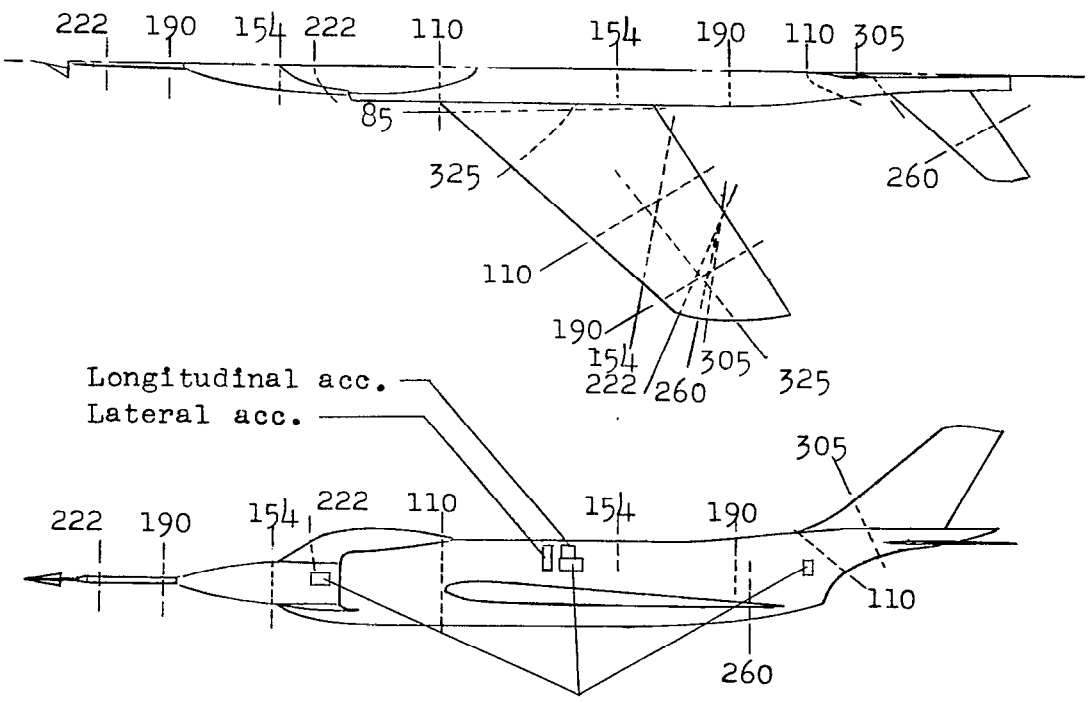

Nodal lines and frequencies at which they occurred.

Figure 3.- Vibration characteristics of the model.

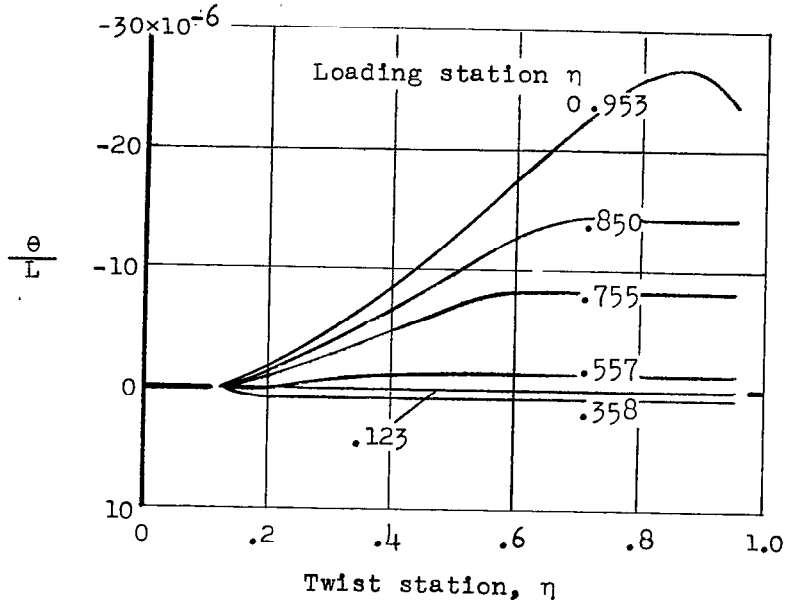

(a) Loading at 25 percent local chord.

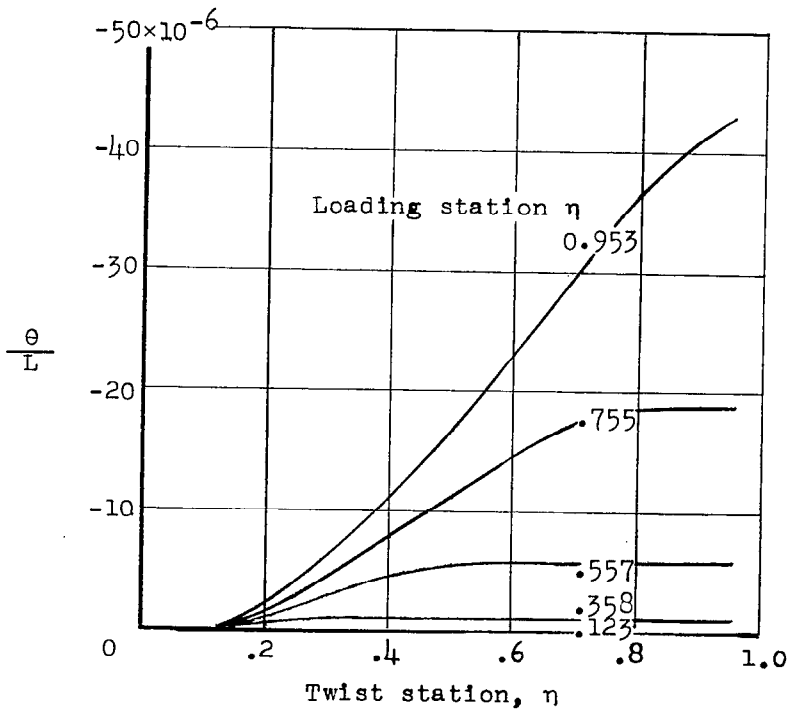

(b) Loading at 50 percent local chord.

Figure 4.- Wing influence coefficients, measured parallel to fuselage center line.

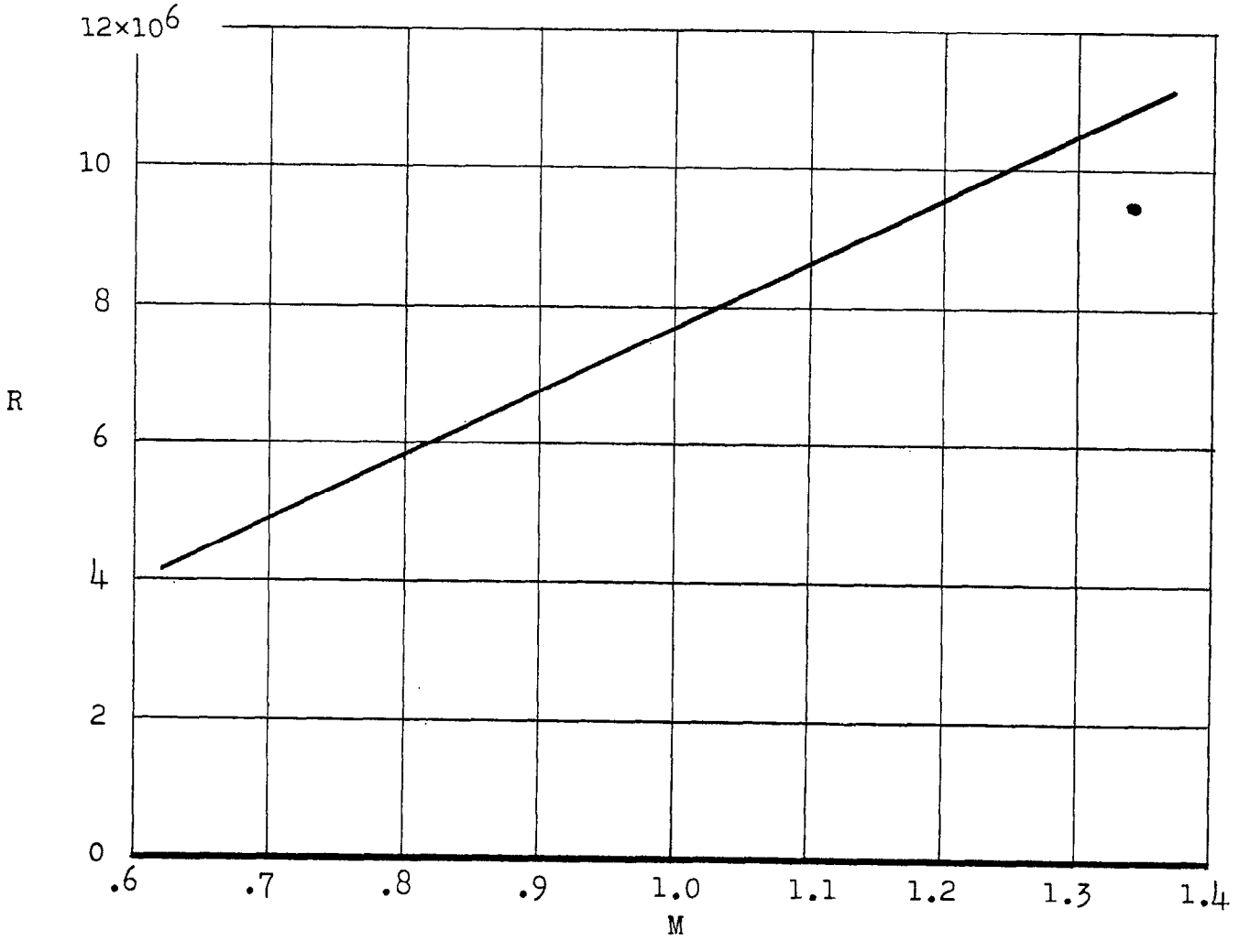

Figure 5.- Test Reynolds number as a function of Mach number.

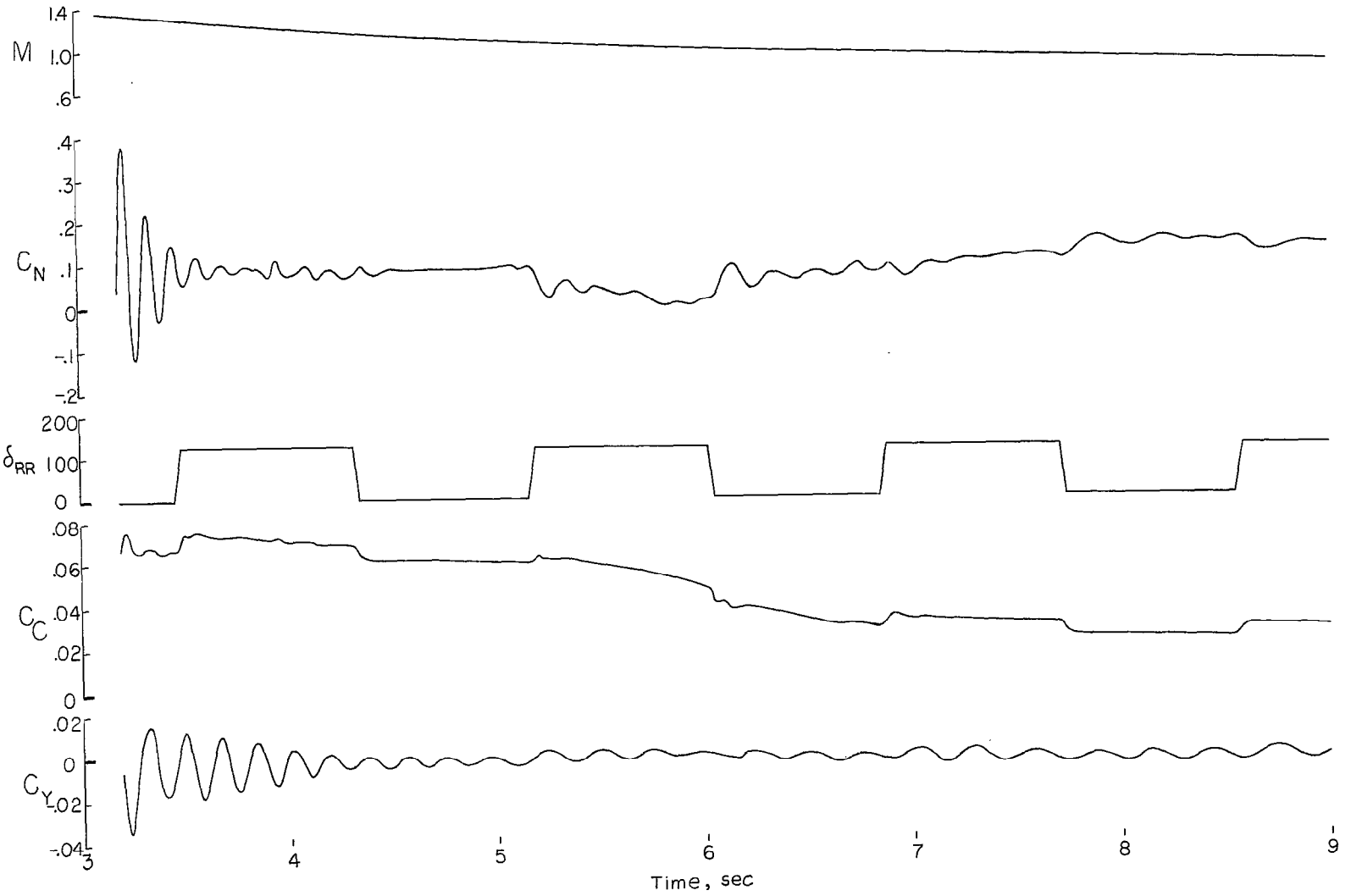

Figure 6.- Time history.

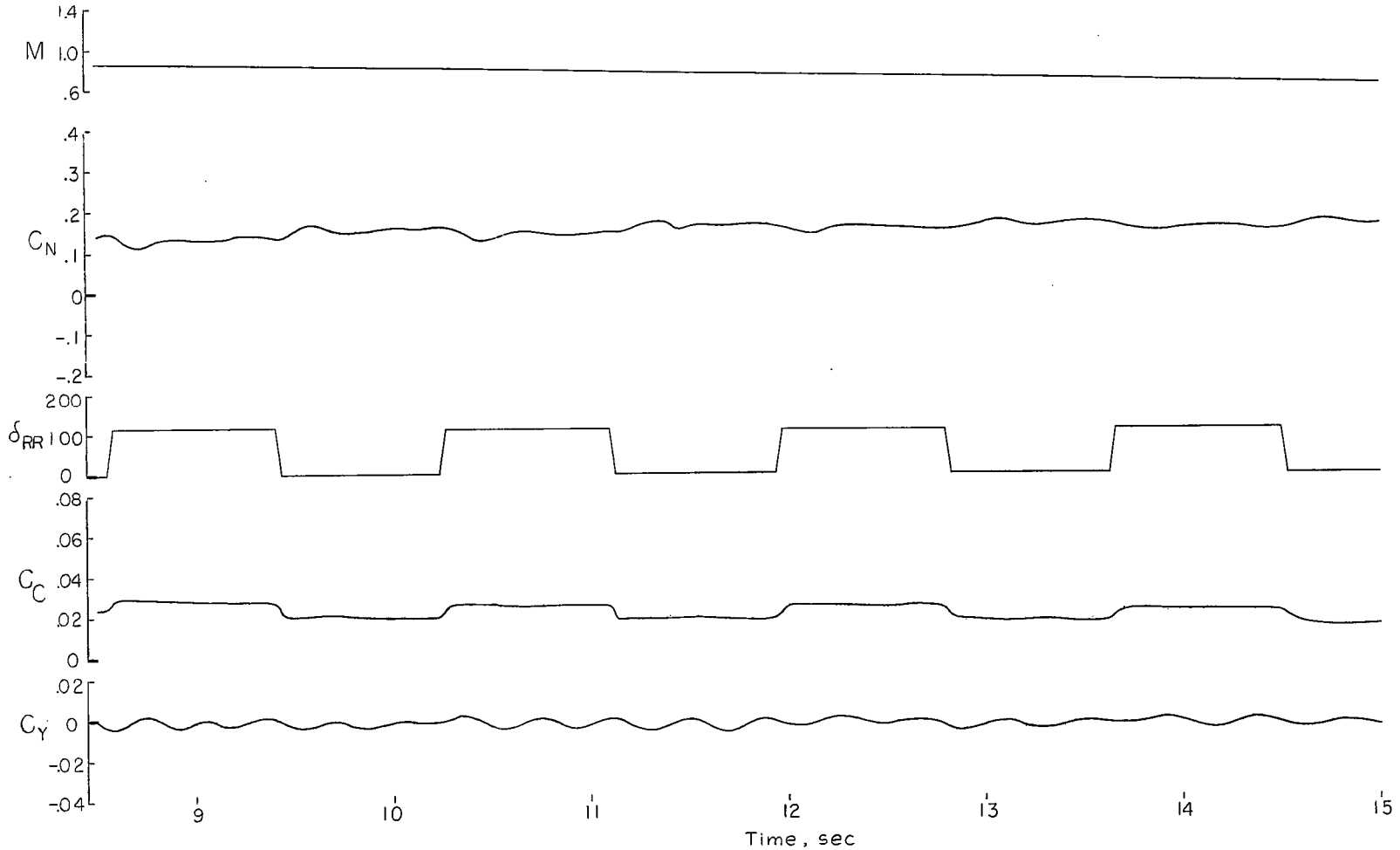

Figure 6.- Concluded.

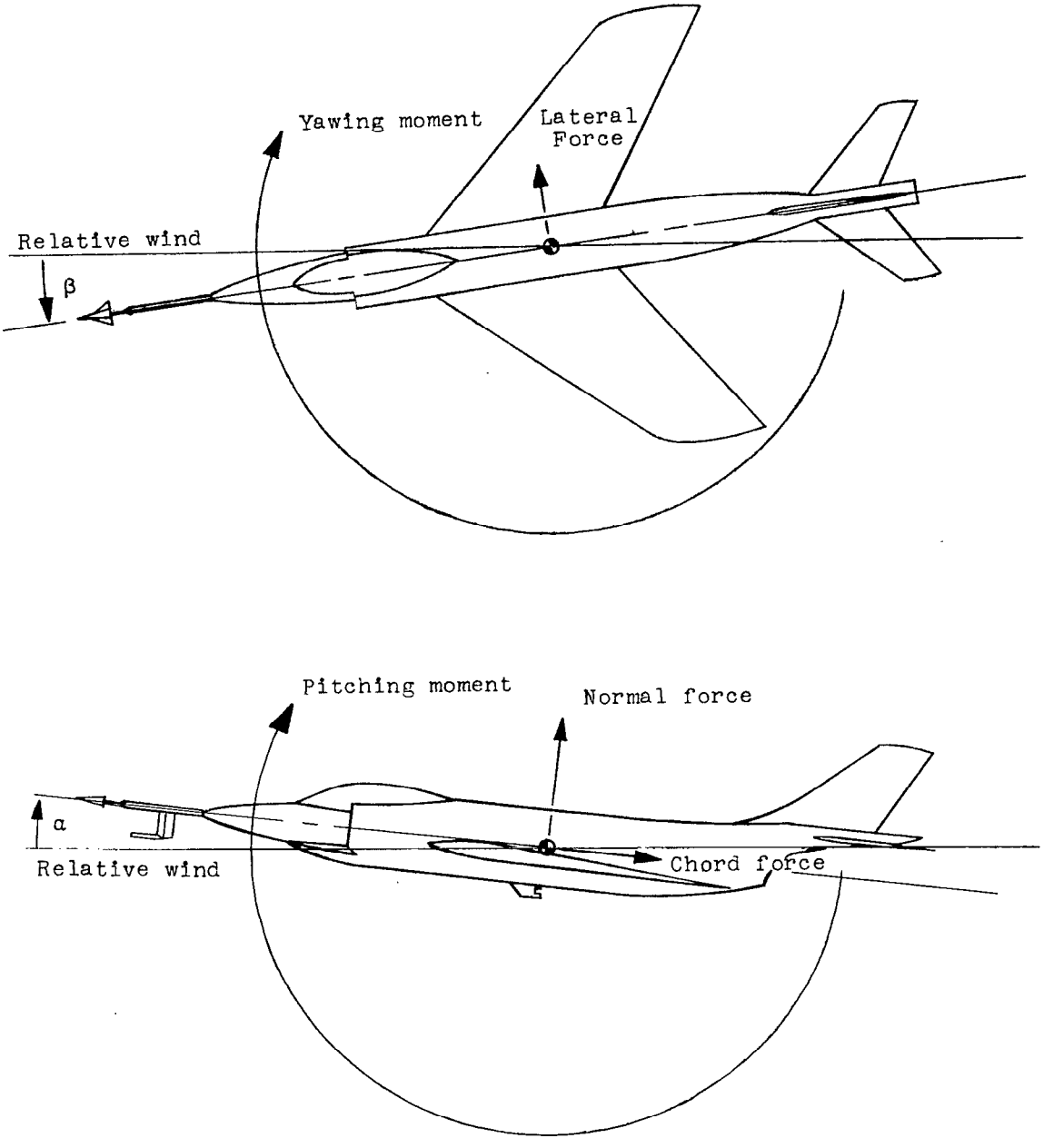

Figure 7.- Positive values of forces, moments, and displacements are indicated by arrows.

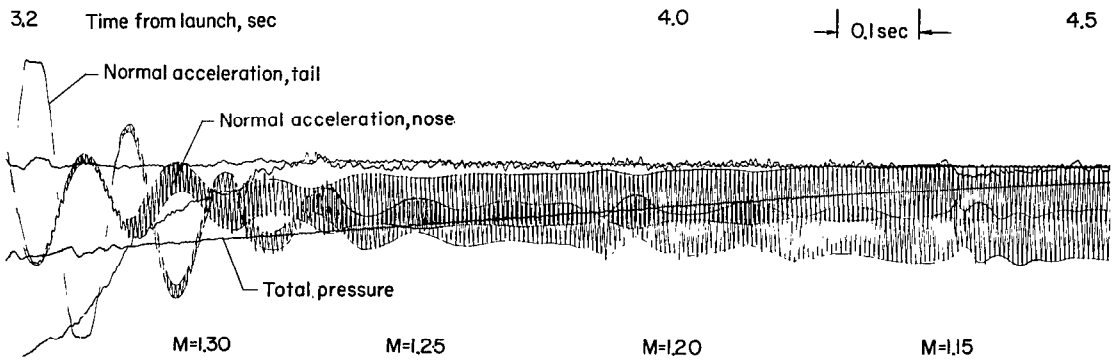

(a) M = 1.37 to 1.14.

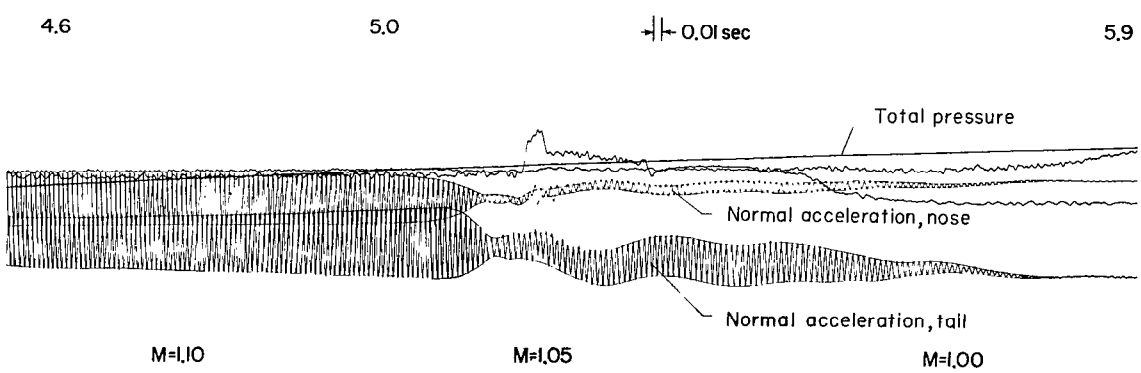

(b) M = 1.14 to 0.98.

Figure 8.- Portion of telemeter record showing flutter oscillation.

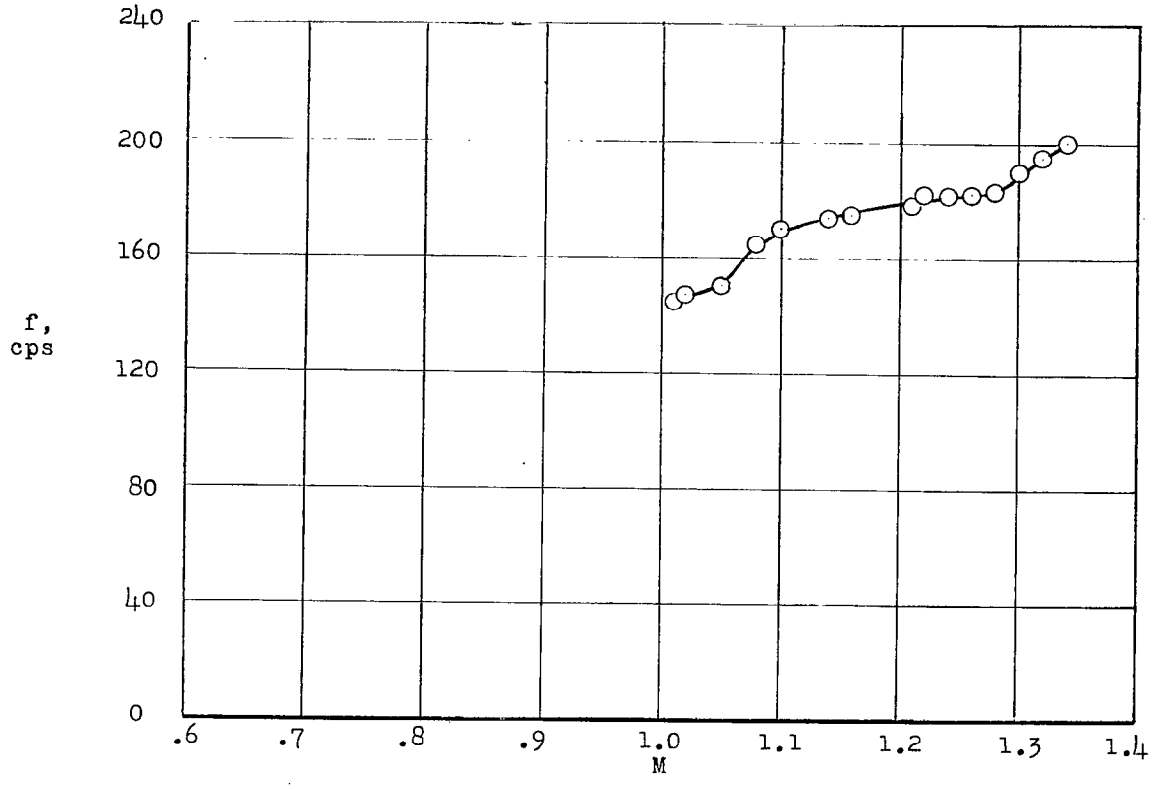

(a) Frequency.

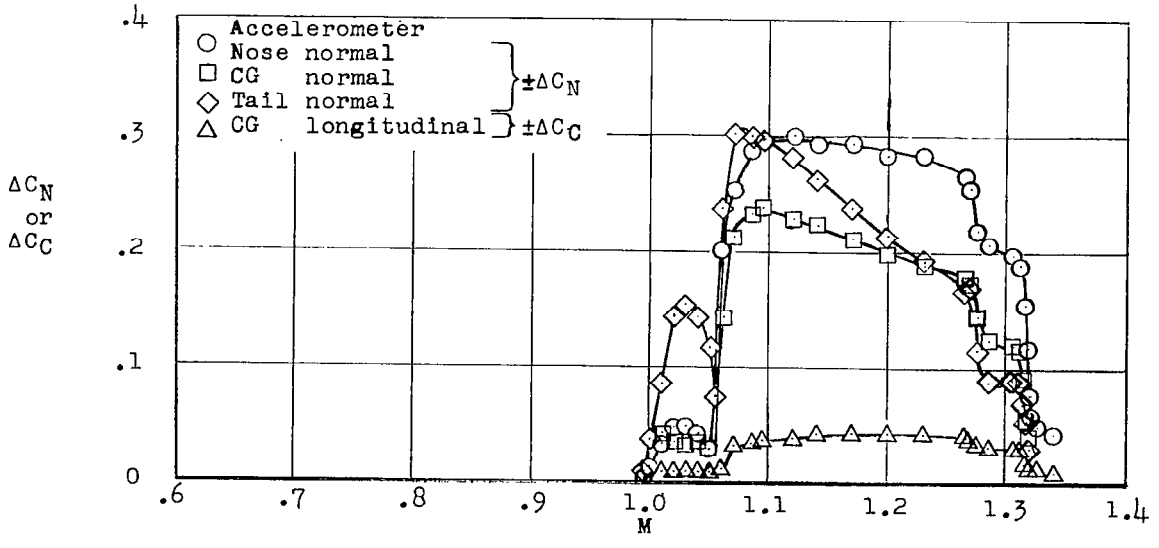

(b) Half amplitude.

Figure 9.- Frequency and half amplitude of the flutter oscillation.

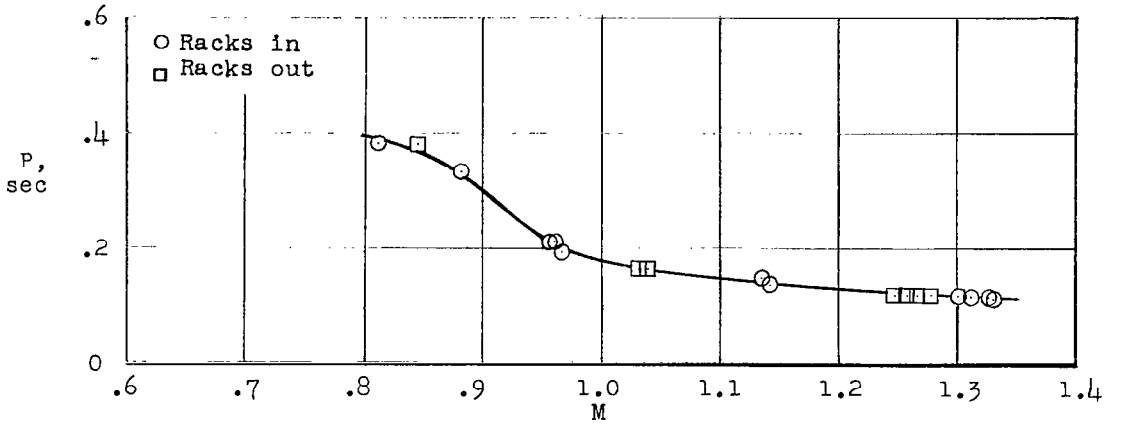

(a) Period of longitudinal motion.

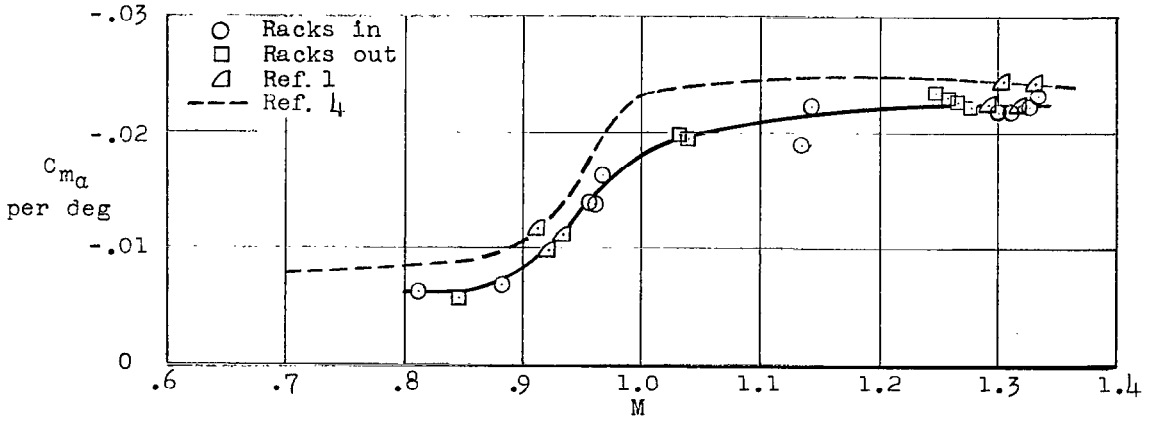

(b) Static-stability derivative C_{m_α}.

Figure 10.- Angle-of-attack stability for center of gravity at 27.9 percent mean aerodynamic chord.

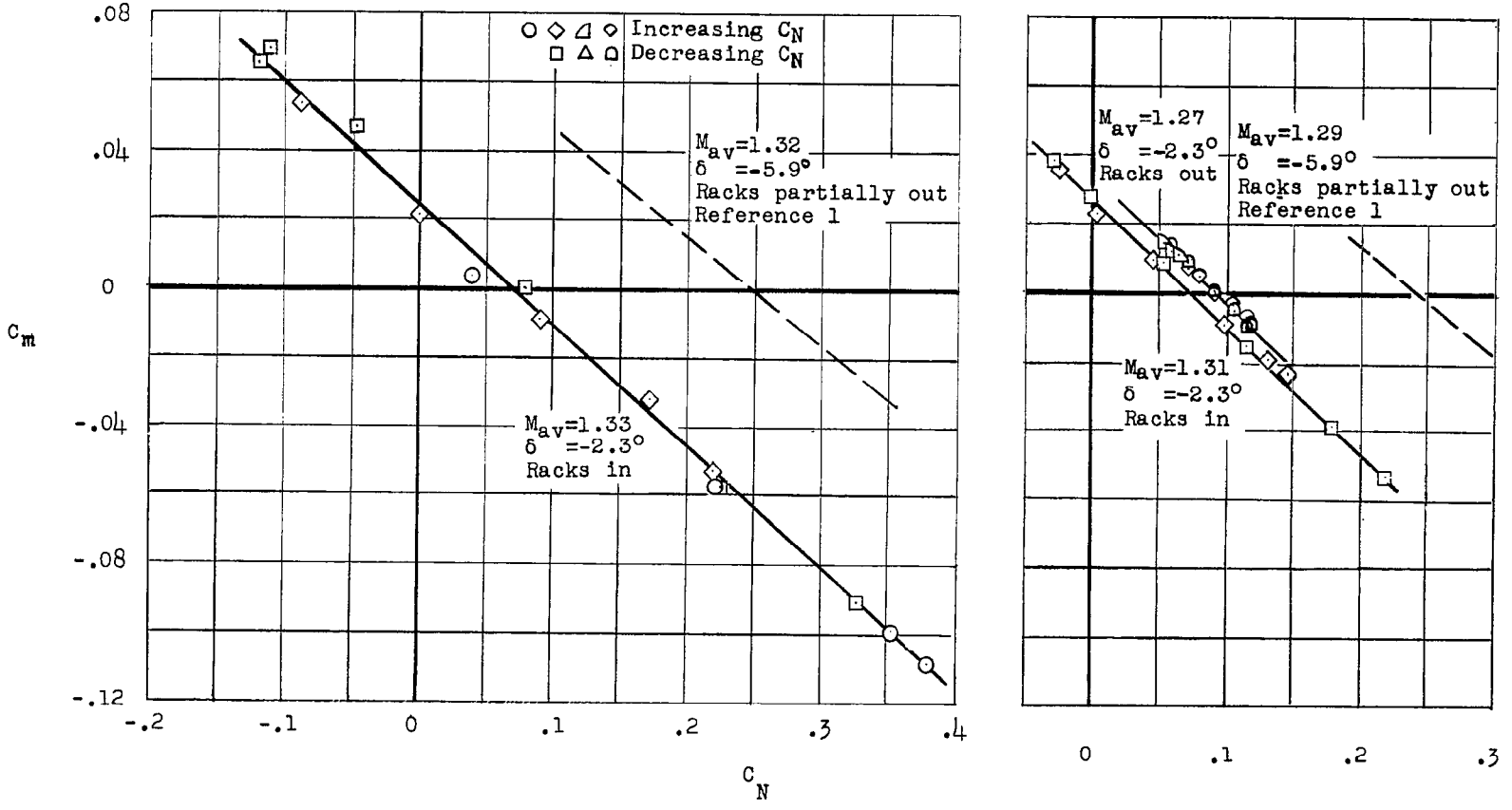

Figure 11.- Static pitching-moment coefficient as a function of normal-force coefficient at several Mach numbers.

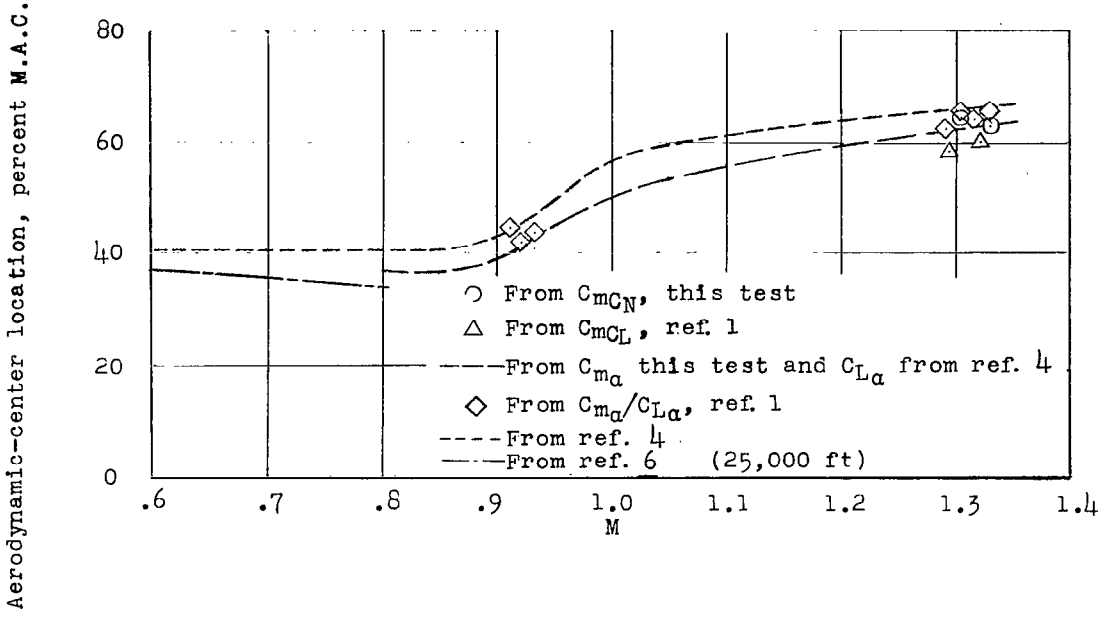

Figure 12.- Variation of aerodynamic-center location with Mach number.

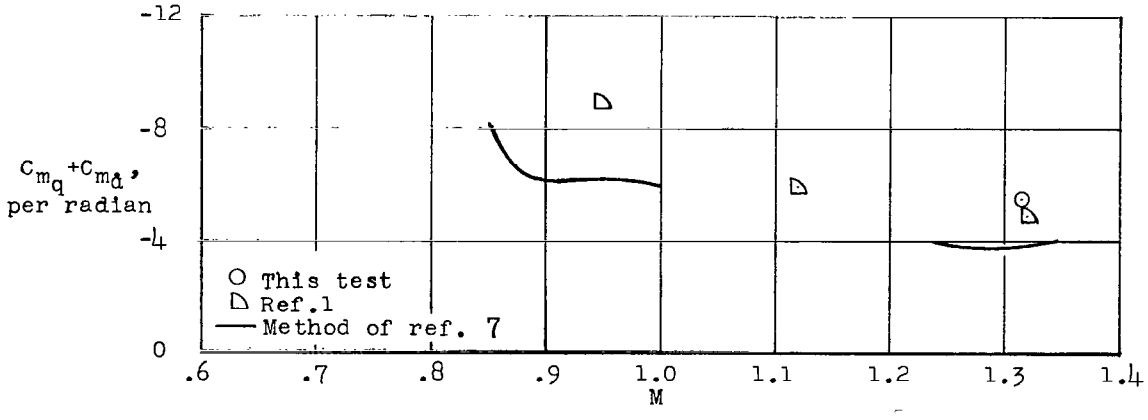

Figure 13.- Dynamic longitudinal-stability parameter $C_{m_q} + C_{m_{\dot{\alpha}}}$.

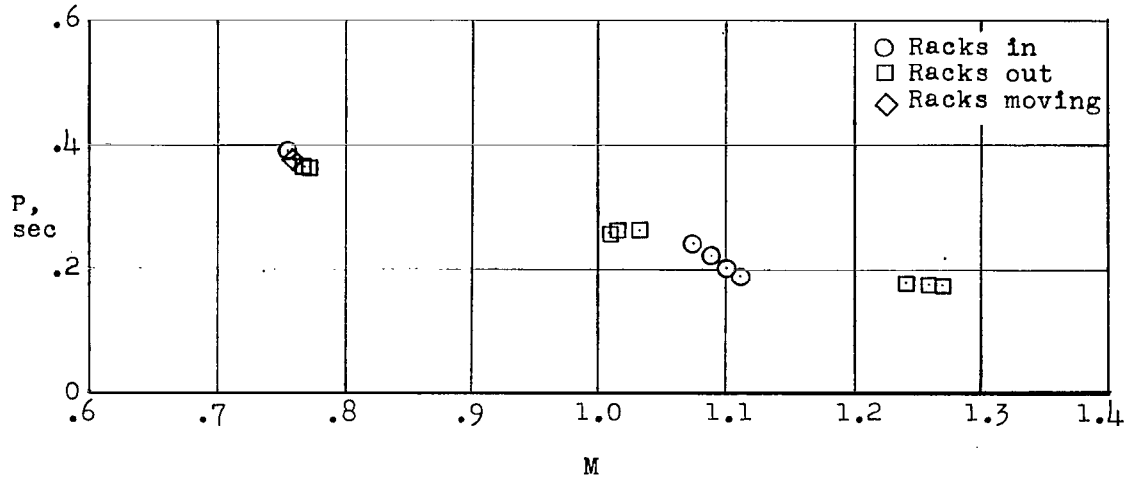

(a) Period of lateral motion.

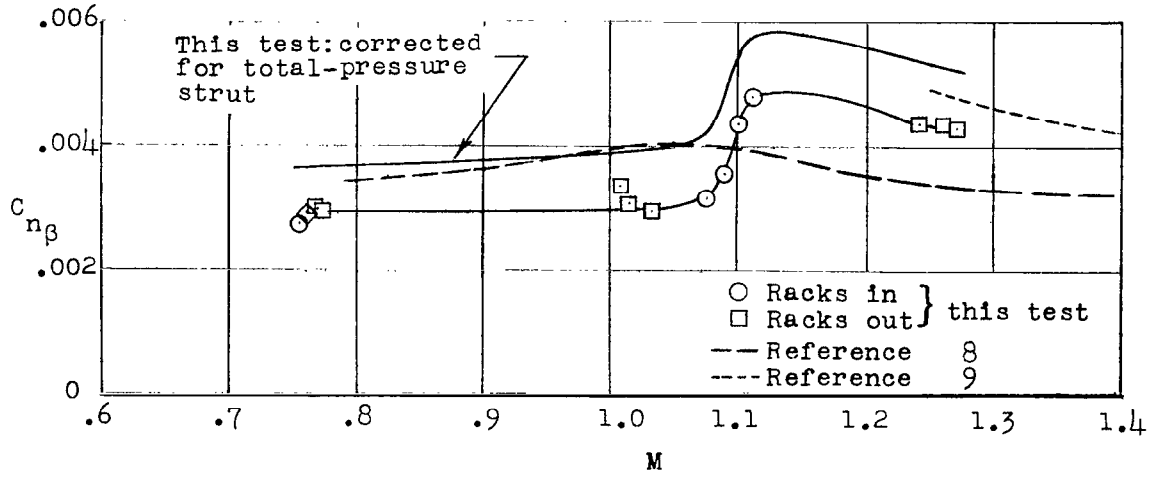

(b) Static-stability derivative C_{n_β}.

Figure 14.- Directional static-stability parameters for center of gravity at 27.9 percent mean aerodynamic chord.

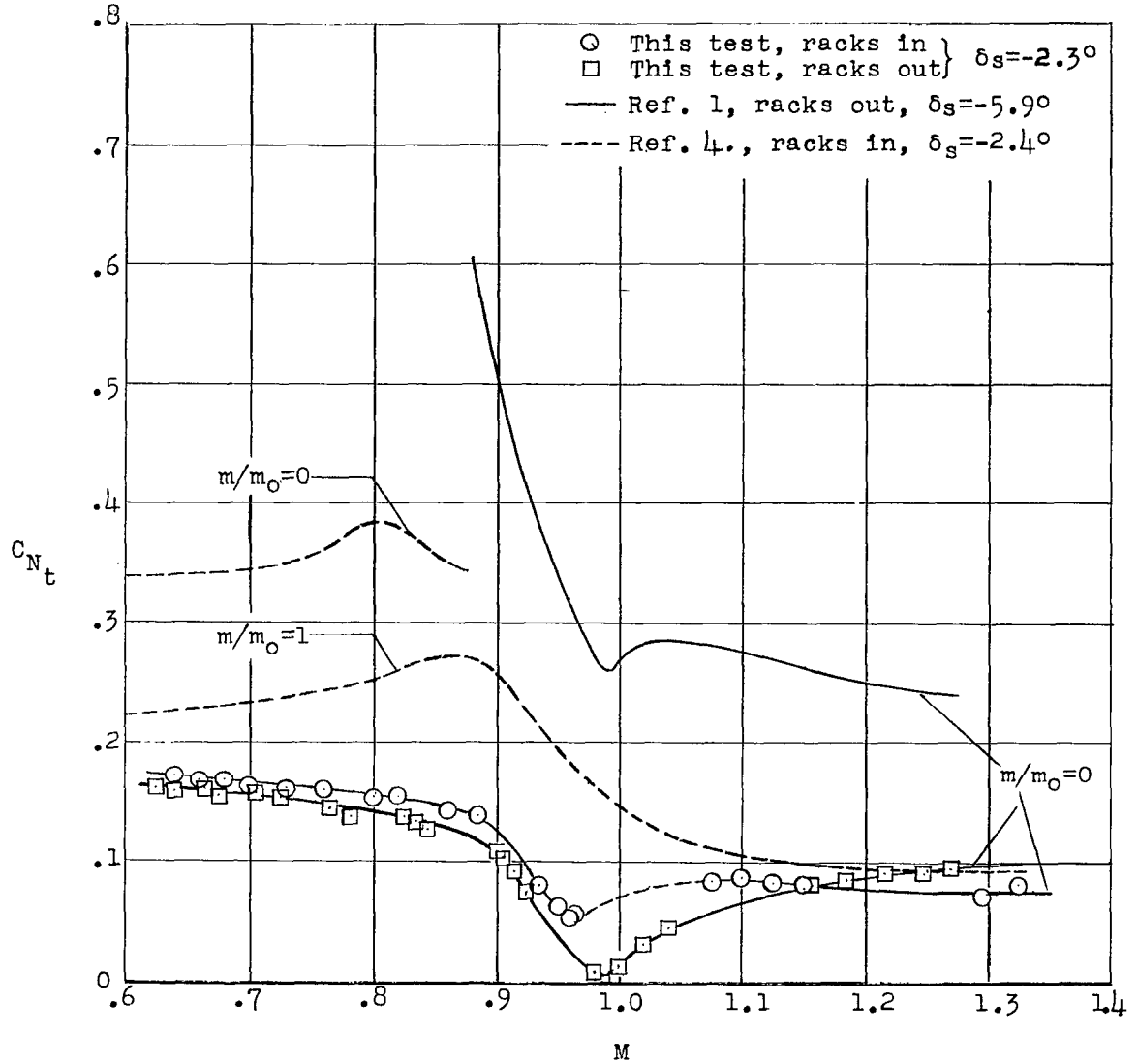

Figure 15.- Normal-force coefficient at trim, for rocket racks in and out.

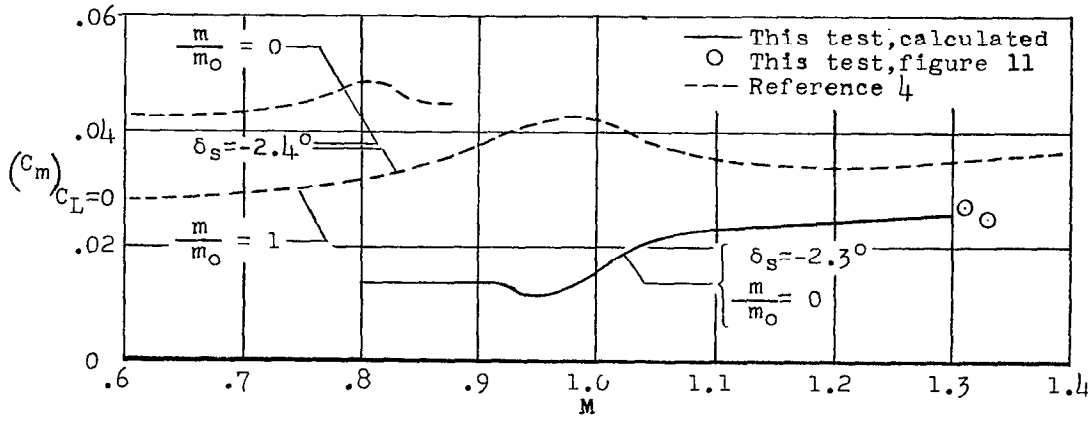

Figure 16.- Pitching-moment coefficient at zero lift.

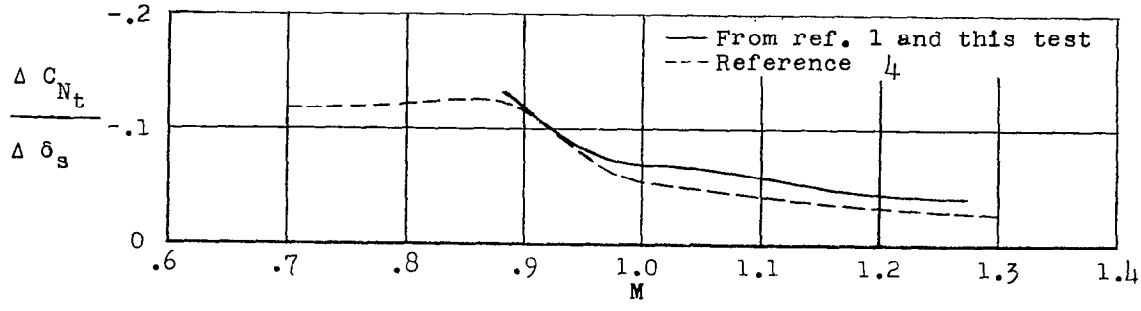

Figure 17.- Stabilizer effectiveness for trim evaluated for racks out.

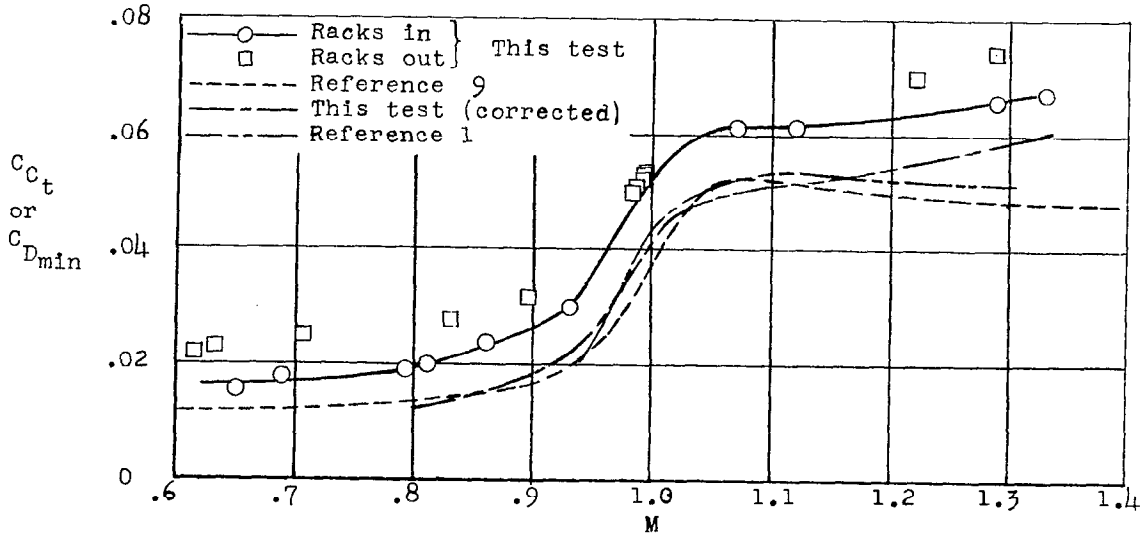

Figure 18.- Chord-force coefficient at trim and minimum drag coefficient.

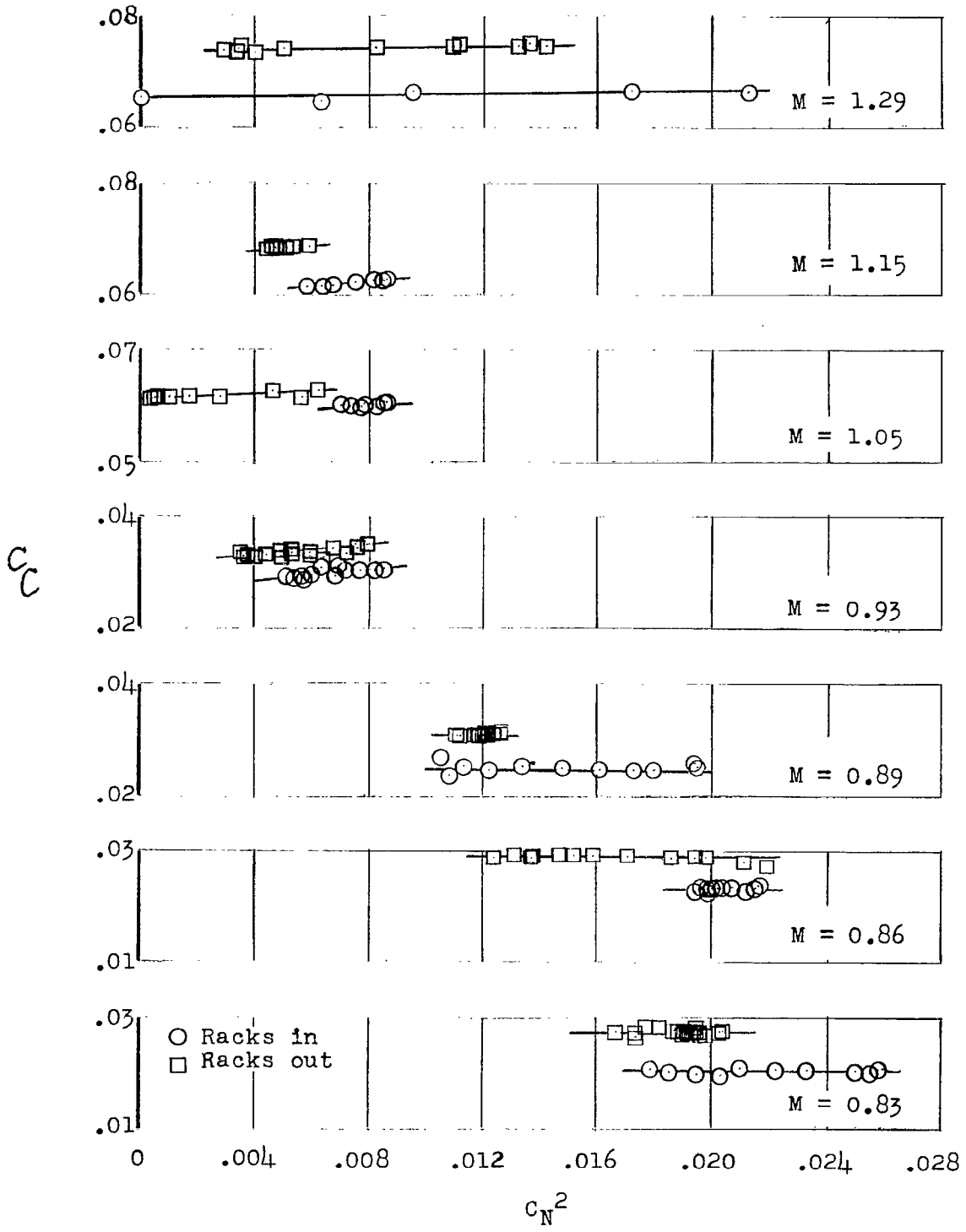

Figure 19.- Effect of rocket racks on the chord-force coefficient at several Mach numbers.

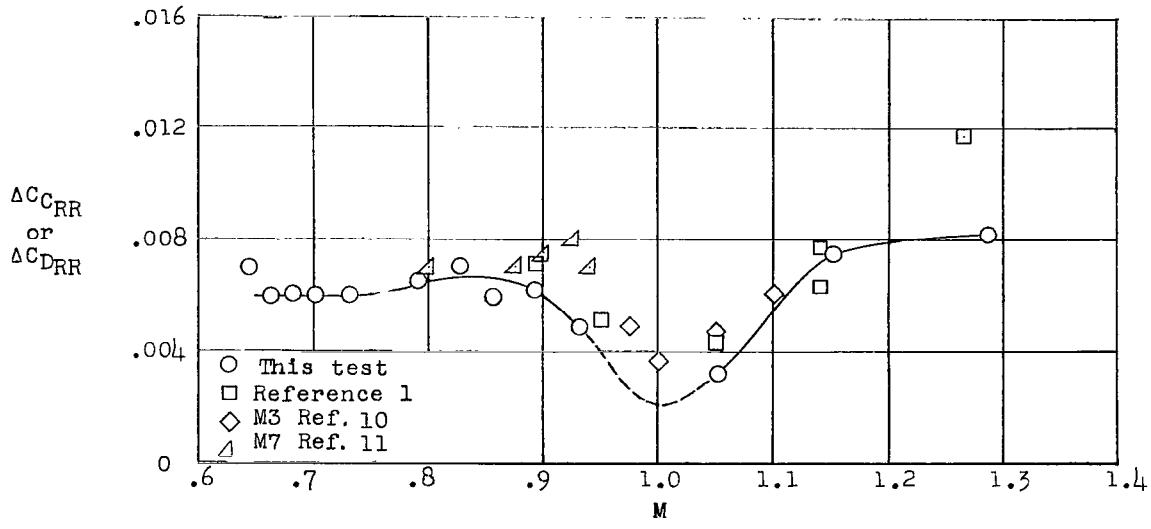

Figure 20.- Increment in drag coefficient due to the racks.

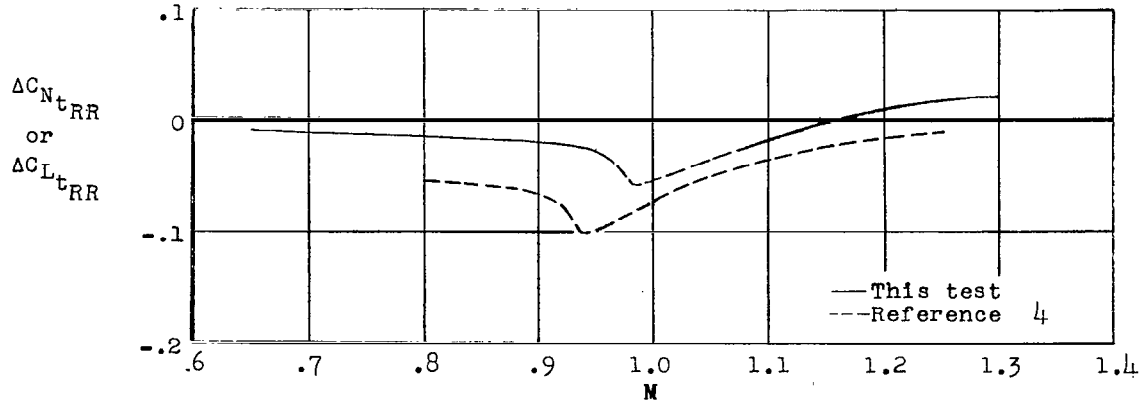

Figure 21.- Effect of rocket racks on trim normal-force coefficient.

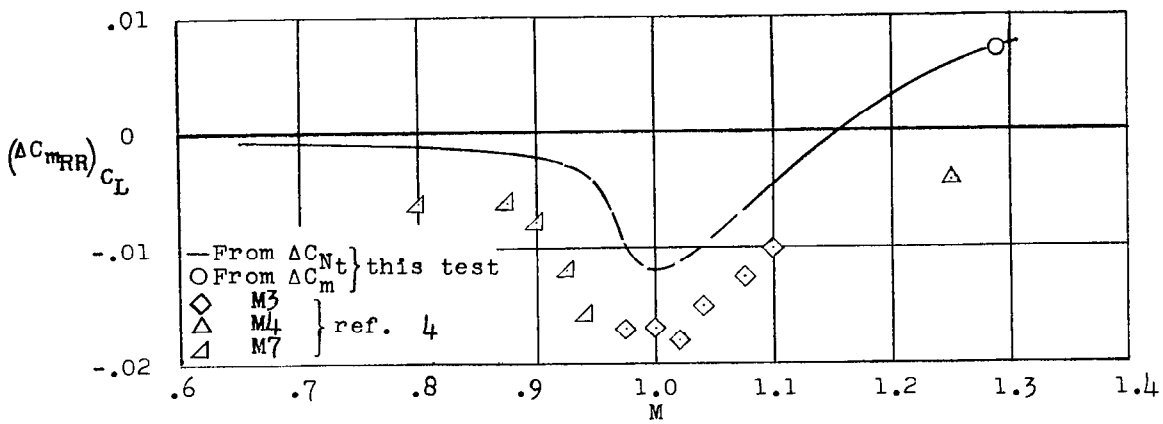

Figure 22.- Effect of rocket racks on pitching-moment coefficient.

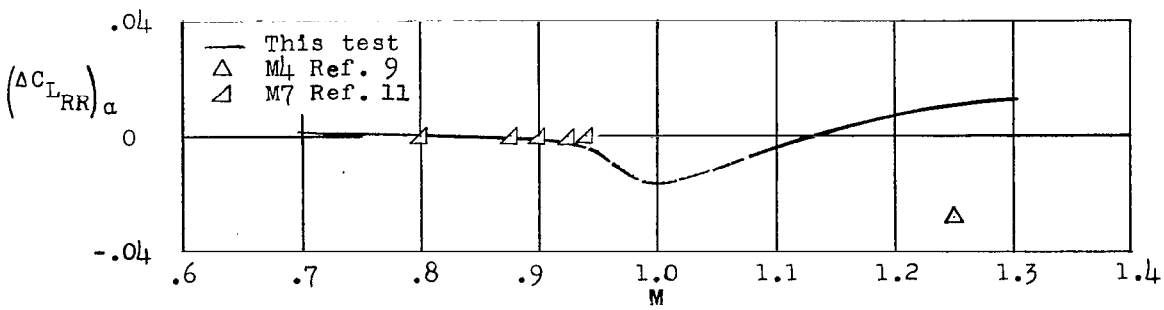

Figure 23.- Effect of rocket racks on lift coefficient.